JOURNAL OF GEOPHYSICAL RESEARCH, VOL. 112, D22S22, doi:10.1029/2006JD008143, 2007

Characterization of the seasonal cycle of south Asian aerosols: A regional-scale modeling analysis

Bhupesh Adhikary,[1,2] Gregory R. Carmichael,[1,2] Youhua Tang,[1] L. Ruby Leung,[3] Yun Qian,[3] James J. Schauer,[4] Elizabeth A. Stone,[4] Veerabhadran Ramanathan,[5] and Muvva V. Ramana[5]

Received 12 October 2006; revised 9 May 2007; accepted 8 June 2007; published 7 November 2007.

[1] The sulfur transport and deposition model (STEM) is used to study the aerosol seasonality, distribution, and composition over south Asia from September 2004 to August 2005. Model predictions of sulfate, black carbon, primary organic carbon, other anthropogenic particulate matter, windblown mineral dusts, and sea salt are compared at two sites in south Asia where yearlong experimental observations are available from the Atmospheric Brown Cloud (ABC) project. The model predictions are able to capture both the magnitude and seasonality of aerosols over Hanimaadhoo Observatory, Maldives. However, the model is not able to explain the seasonality at the Kathmandu Observatory; but the model does capture Kathmandu's observed annual mean concentration. The absence of seasonal brick kiln emissions within Kathmandu valley in the current inventory is a probable reason for this problem. This model study reveals high-anthropogenic aerosol loading over the Ganges valley even in the monsoonal months, which needs to be corroborated by experimental observations. Modeling results also show a high dust loading over south Asia with a distinct seasonality. Model results of aerosol monthly composition are also presented at five cities in south Asia. Total and fine-mode monthly aerosol optical depth along with contribution from each aerosol species is presented; the results show that the anthropogenic fraction dominates in the postmonsoon and the early dry season with major contributions from sulfate and absorbing aerosols. Model sensitivity studies of dry deposition velocity and wet scavenging efficiency show that model improvements are needed in the treatment of carbonaceous aerosol dry and wet removal processes. Modeled SO_2 conversion rate constrained with sulfate observations at Hanimaadhoo suggests the need to increase model sulfate production rate during the dry season to account for probable sulfate production via heterogeneous pathways.

Citation: Adhikary, B., G. R. Carmichael, Y. Tang, L. R. Leung, Y. Qian, J. J. Schauer, E. A. Stone, V. Ramanathan, and M. V. Ramana (2007), Characterization of the seasonal cycle of south Asian aerosols: A regional-scale modeling analysis, *J. Geophys. Res.*, *112*, D22S22, doi:10.1029/2006JD008143.

1. Introduction

[2] Aerosols absorb and reflect solar radiation reaching the Earth's surface; hence they play an important role in the radiation budget of the Earth. Variations in the radiation budget can lead to perturbations on the hydrological cycle [*Ramanathan et al.*, 2005, 2001a] and the photosynthesis rate of plants [*Chameides et al.*, 1999]. Furthermore, positive correlations have been established by epidemiologists between ambient aerosol concentration and human health endpoints [*Pope et al.*, 2002, 2006].

[3] Aerosol characterization studies over south Asia are rather recent. The Indian Ocean Experiment (INDOEX) studied aerosol characteristics over south Asia [*Ramanathan et al.*, 2001b]. INDOEX documented the existence of haze over the Indian subcontinent and quantified the impact on the solar radiation budget over the region. After the INDOEX intensive field campaign, there has been substantial experimental research to characterize aerosol over the Indian subcontinent [*Carrico et al.*, 2003; *Moorthy et al.*, 2005; *Rastogi and Sarin*, 2005; *Sumanth et al.*, 2004]. These experimental studies point out high aerosol loadings over

[1]Center for Global and Regional Environmental Research, University of Iowa, Iowa City, Iowa, USA.
[2]Department of Chemical and Biochemical Engineering, University of Iowa, Iowa City, Iowa, USA.
[3]Pacific Northwest National Laboratory, Richland, Washington, USA.
[4]Environmental Chemistry and Technology Program, University of Wisconsin-Madison, Madison, Wisconsin, USA.
[5]Center for Atmospheric Sciences, SCRIPPS Institute of Oceanography, University of California at San Diego, La Jolla, California, USA.

0148-0227/07/2006JD008143$09.00

both rural and urban sites with significantly different local aerosol characteristics.

[4] *Carrico et al.* [2003] observed high carbonaceous and dust aerosol loading at two remote Himalayan sites; they explain their dust observations on the basis of long-range transport, possibly as far as from the Saharan deserts. *Moorthy et al.* [2005] analyzed near-surface aerosol characteristics over peninsular India during February–March 2004. Their results show significantly higher aerosol loading along the coastal and near-urban locations versus the semiarid interior continental regions. *Moorthy et al.* [2005] also show that fine-mode aerosol contribute more than 50% of the total aerosol mass in the coastal regions, while the interior regions showed abundance of coarse-mode particles. *Babu et al.* [2002] observed high contribution of black carbon (BC) aerosol mass to the total aerosol mass at Bangalore (an urban location) which was significantly higher than that reported during the INDOEX campaign, while *Sumanth et al.* [2004] observed significantly lower contribution of BC mass to total aerosol mass over the Bay of Bengal when compared to the INDOEX findings. Recent studies have also debated the sources of carbonaceous aerosol over the Indian subcontinent: fossil fuels [*Mayol-Bracero et al.*, 2002; *Novakov et al.*, 2000] versus biofuels [*Parashar et al.*, 2005; *Venkataraman et al.*, 2005].

[5] To further characterize the nature of south Asian aerosols and their impacts on the environment, the United Nations Environmental Program (UNEP) and the Center for Clouds, Chemistry and Climate (C^4) launched an international project called the Atmospheric Brown Cloud (ABC) project [*UNEP and C*^{4}, 2002]. The project has set up long-term experimental observatories throughout south Asia and recently completed two intensive field campaigns. The first campaign, ABC–Postmonsoon Experiment (ABC-APMEX), was conducted over the Maldives in October–November 2004. During the ABC-APMEX study period the winds change direction from southwesterly to north and northeasterly in transition to the winter monsoon, bringing pollution from the Indian subcontinent and Southeast Asia to the Indian Ocean and Arabian Sea. Through these activities, aerosol observations are available for a full year. This provides a good opportunity to examine the anthropogenic aerosol loading in the atmosphere over this region.

[6] One component of the ABC project is to apply, evaluate, and improve the capacity of chemical transport models (CTMs) to predict aerosol distributions in Asia. In the past several years, global [*Chung and Seinfeld*, 2002; *Koch*, 2001; *Liousse et al.*, 1996; *Penner et al.*, 1993; *Reddy et al.*, 2004] and regional [*Minvielle et al.*, 2004a, 2004b; *Uno et al.*, 2003a; *Zhang*, 2004] models have studied the effects of major anthropogenic aerosols in the Asian atmosphere. However, global models do not have the finer grid resolution required to study the aerosol effect on a regional scale, and past regional models have been run only for short intensive field campaigns, hence limiting the study of seasonal variation. In support of the ABC-APMEX we provided real-time forecasts of aerosol and trace gases using the STEM model in aid of flight planning as well as understanding and analysis of the experimental observations. This model has been extensively applied and evaluated in the east Asian applications [*Carmichael et al.*, 2003; *Guttikunda et al.*, 2005; *Tang et al.*, 2004]. This represents the first evaluation of the STEM model to south Asian application.

[7] In this paper we have applied this model to study the seasonal variation in aerosol composition in south Asia. We evaluate the model by comparing the model predictions to observations of aerosol composition at two ABC sites, Hanimaadhoo Climate Observatory (HCO), Maldives, and Kathmandu Observatory (KTM), from September 2004 to August 2005. The STEM model is then used to elucidate the seasonality and spatial distribution of the major south Asian aerosols, namely black carbon (BC), organic carbon (OC), sulfate, dust, and sea salt. We then characterize and discuss the seasonal cycle of aerosol composition at various sites throughout south Asia.

2. Model Overview

2.1. STEM Model

[8] Aerosol distributions in south Asia were simulated using the sulfur transport and deposition model (STEM). The STEM model has been successfully used for aerosol characterization studies in Asia. For example, the model was used to analyze BC and sulfate aerosol distributions during the TRACE-P intensive field phase [*Carmichael et al.*, 2003]. The STEM model was also used to study the impact of dust on regional chemistry during the Ace-Asia experiment [*Tang et al.*, 2004]. The STEM modeling domain size, horizontal and vertical resolution and the map projection is the same as that of the MM5 modeling domain which is discussed in section 2.2.

[9] For this study the STEM model used fixed top and lateral boundary conditions, the details of which have been discussed previously [*Carmichael et al.*, 2003]. It has been shown that a regional model coupled with top and lateral boundary conditions from a global model greatly enhances model skill *Tang et al.*, 2007. However, since no global model forecasts were available for this study, the boundary conditions were set to a typical clean marine environment over the oceans and clean rural environment over land [*Uno et al.*, 2003b].

[10] Both hydrophobic and hydrophilic BC and OC are analyzed with an initial 80/20 percent split (for BC) and 50/50 percent split (for OC), respectively, as reported in previous modeling studies [*Chung and Seinfeld*, 2002; *Reddy and Boucher*, 2004]. Both BC and OC are allowed to age and are converted to hydrophilic tracers with a fixed aging rate of 7.1E-6 s^{-1} as previously reported in the literature [*Cooke and Wilson*, 1996]. Sulfate is calculated using SO_2 conversion parameterization used during analysis of the ACE-Asia experiment with rates between 1 and 10% per h [*Uno et al.*, 2003b].

[11] The dry deposition scheme for aerosols is based on the resistance in series parameterization work of *Walcek et al.* [1986] originally developed by *Wesley and Hicks* [2000] in 1977, and the values vary with land cover and meteorological conditions. The majority of studies on dry deposition have been conducted on sulfate aerosols; however, there are also some limited studies on carbon deposition. *Cadle and Dasch* [1988] estimated the dry deposition velocity of particulate carbon on snow surface at a rural site in northern Michigan; their experimentally deduced values range from 0.05 to 0.9 cm s^{-1}. In this study, dry deposition velocities of

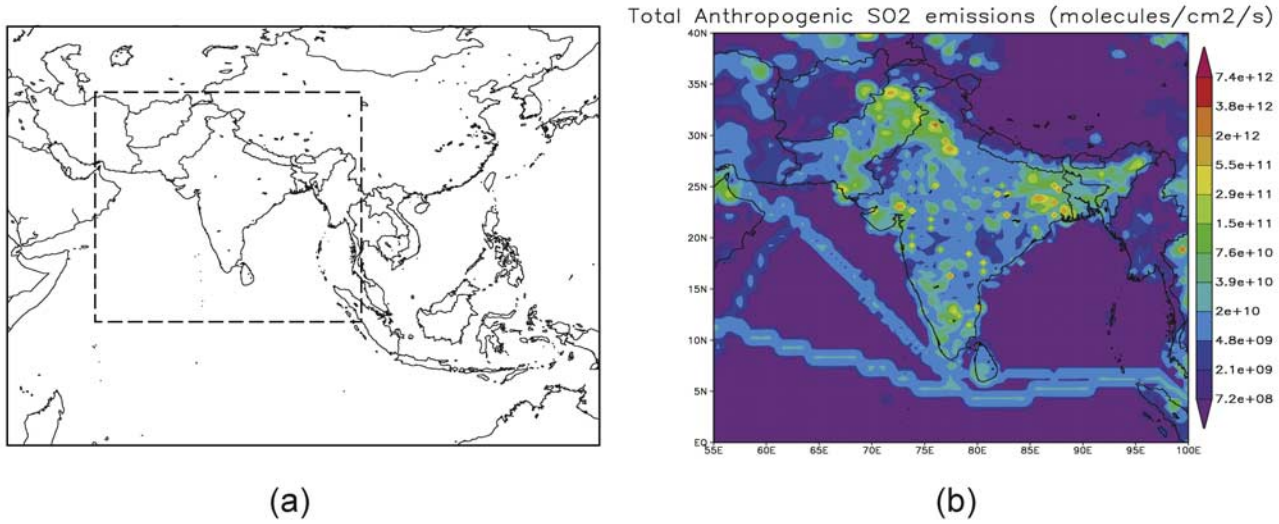

Figure 1. (a) Modeling domain and analysis domain (dashed line) and (b) the spatial distribution of SO_2 emissions used in the study for south Asia.

BC, OC, windblown dust and sea salt, $PM_{2.5}$, and PM_{10} were scaled to sulfate aerosol dry deposition; BC and OC have the same dry deposition velocity as sulfate, while coarse-mode aerosols such as sea salt and dust have dry deposition values 3 to 5 times that of sulfate (depending on size). Wet scavenging was modeled as a loss rate that varies with precipitation rate, which is a prognostic variable of MM5, as described by *Uno et al.* [2003a].

2.2. Meteorology Model: MM5

[12] The Penn State/NCAR Mesoscale model MM5 [*Grell et al.*, 1995] was used to generate meteorological conditions for driving the aerosol transport model. For this study a single MM5 domain with a horizontal resolution of 50 km by 50 km was used. Geographically, the domain centers at 90°E and 18°N and covers 40°E to 140°E and 21°S to 50°N with 219 by 179 grid cells. The model has 23 vertical layers with a model top at about 14 km. Figure 1a illustrates the modeling domain and the analysis domain. The simulation used a similar set of physics parameterizations tested by *Leung et al.* [2003] and *Qian and Leung* [2007] for the United States and east Asia.

[13] The MM5 model was driven by the large-scale conditions from the NCEP/NCAR global reanalysis and run from 1 September 1998 to 30 November 2005. Only the period from 1 August 2004 to 31 August 2005 that covers both ABC field campaigns is used in this study to analyze the seasonal distribution. Since the model domain is relatively large, the lateral boundary conditions do not sufficiently constrain the atmospheric circulation in the regional simulation for aerosol transport modeling over a long time period. Therefore data assimilation was applied using simple nudging to constrain the atmospheric circulation (including temperature and winds) by the large-scale conditions supplied by the NCEP/NCAR global reanalysis throughout the model domain (above the simulated atmospheric boundary layer) and simulation period. The transition from the southwest summer monsoon to the northeast winter monsoon circulation is well captured during the ABC-APMEX. This is important for simulating aerosols over the Arabian Sea and the Indian Ocean that originate from the Indian subcontinent during the dry season. At 50 km spatial resolution the regional simulation provides a better description of orography (such as the western Ghats and land-sea contrast) and its impact on winds and precipitation compared to the global reanalysis. This is supported by comparisons of the observed and simulated spatial distribution and diurnal timing of rainfall averaged over the 7-a simulation period (not shown).

2.3. Emissions Inventory

[14] The fossil fuel emissions of SO_2, BC, OC, other $PM_{2.5}$, and other PM_{10} (i.e., those non-BC, non-OC primary particulate emissions, e.g., those from construction) used in the analysis are those from the inventory developed for the TRACE-P and ACE-Asia campaigns [*Streets et al.*, 2003]. The emissions inventory from *Streets et al.* [2003] was developed for the year 2000 and is gridded at a spatial resolution of 30 s $\times$ 30 s using exact locations of large point sources and GIS distribution of urban/rural population and transportation network. The domain stretches from Indonesia in the south to Mongolia in the north and from Pakistan in the west to Japan in the east. Since the model domain for this study is bigger than the TRACE-P domain, the Emission Database for Global Atmospheric Research (EDGAR) was used for the rest of the domain [*Olivier and Berdowski*, 2001]. The biomass burning emissions inventory for BC and OC was taken from *Reddy and Boucher*'s [2004] climatological (1997–2001) global estimates. Table 1 provides the summary of anthropogenic (fossil plus biofuel) emissions of SO_2, BC, and OC for the south Asian countries. Table 2 presents average monthly BC and OC biomass emissions for the south Asian region from 0 to 40°N and 55–100°E.

[15] Figure 1b shows the spatial distribution of SO_2 emissions for the study domain. The emissions of SO_2 in the Indian subcontinent are high in north India along the Ganges plain, which extends to east India around the Kolkata region; Figure 1b also shows high point source emissions coming mainly from large power plants and

Table 1. Summary of Anthropogenic Emissions[a]

Region	SO_2	BC	OC
Bangladesh	131.1	39.0	187.6
Bhutan	5.3	1.3	6.1
India	5462.2	517.1	2189.6
Nepal	31.9	17.2	82.7
Pakistan	1409.8	76.5	316.0
Sri Lanka	55.7	8.0	33.5
South Asia total	7096.0	659.1	2815.6
Myanmar	31.1	24.8	112.6
Total	7127.0	683.9	2928.2

[a]Trace-P annual SO_2 emissions. Units: Gg/a. BC is black carbon and OC is organic carbon.

industries which are scattered all over India. BC and OC also show similar spatial emission distributions (not shown). During the biomass burning seasons of March and April, BC and OC emissions (not shown) are mainly from the Indian states of Maharashtra, Andhra Pradesh, Karnataka, and Tamil Nadu. The emissions inventory used in this study (not shown) illustrates that the total BC/OC ratios over south Asia are rather uniform spatially and vary seasonally only with the contribution from biomass burning. Quantitatively, the BC/OC ratios are between 0.2–0.3 over the Indian subcontinent with higher ratios along the western coast of India and Pakistan versus the interior and the eastern coastline. The ratio varies from 0.1–1 over China and the Pacific where more regional variations are observed.

[16] Sea salt emissions were calculated online on the basis of the parameterization of *Gong* [2003]. Sea salt emissions are calculated for four size bins from 0.1 μm to 10 μm; however, during aerosol transport the size distribution is reduced to fine and coarse mode with fine mode being less than 2.5 μm and coarse mode being less than 10 μm but greater than 2.5 μm. Dust emissions were calculated online on the basis of the method discussed by *Tang et al.* [2004]. Dust emission, transport, and deposition are modeled using two size bins: submicron (diameter < 1 μm) and supermicron (1 μm < diameter < 10 μm).

3. Results and Discussion

[17] To investigate the seasonal cycle of aerosols in south Asia, the STEM model was run for 12 months from September 2004 to August 2005. This period covers the observations at Hanimaadhoo Climate Observatory (HCO) and Kathmandu Station (KTM). Experimental observations of aerosols and methodologies are explained in detail in the accompanying articles [*Ramanathan et al.*, 2007; *Stone et al.*, 2007]. The model was allowed to spin up for the month of August 2004, and then comparisons with observations were made from September 2004 onward. The STEM model predictions for BC, OC, sulfate, windblown dust and sea salts, other $PM_{2.5}$, and other PM_{10} were analyzed. We first compare the seasonal variations in observations and predicted aerosol composition at HCO and KTM sites. We then discuss the major factors controlling the seasonal cycle and then extend the analysis to the south Asian region as a whole.

3.1. Seasonality of Aerosols at the Hanimaadhoo Observatory

[18] Figure 2 illustrates the temporal distribution of observed and modeled (fine-mode, nominally 2.5 μm) sulfate, BC, and OC. The anthropogenic aerosol loadings over HCO in this study show a distinct seasonality. For the discussions that follow we classify the seasonal cycle into three periods: the postmonsoon (October–November); the dry (December–April); and the monsoon (June–September) [*Ramana and Ramanathan*, 2006]. As shown in Figure 2, the aerosol concentrations are at a minimum in the monsoon period, rise rapidly and reach a maximum during the postmonsoon period, and they remain elevated, but slowly decline in strength during the dry period. The monsoonal months show a minimum anthropogenic aerosol loading.

[19] Quantitatively, Figure 2a (red squares) shows that the observed sulfate concentration is less than 2.0 $\mu g/m^3$ at HCO when the measurements start in October 2004. The observations show a rise toward late November with concentrations reaching as high as 12.0 $\mu g/m^3$. Elevated sulfate concentrations are observed until the end of December when observations were suspended. The measurements resumed again in late February 2005 where the sulfate aerosol concentrations were still elevated but showed a declining trend, reaching around 3.0 $\mu g/m^3$ by May 2005. The next observation period started in June and ended in early August. During this time the observed sulfate concentration was fairly constant with values around 1.0 $\mu g/m^3$.

[20] The model-predicted values are also shown in Figure 2a. The model predictions capture the general features of the seasonal cycle and do a good job in predicting the peak values and the background levels. However, sulfate levels are systematically underpredicted during the dry season. This underprediction could be due to a systematic underprediction in the SO_2 emissions or due to underprediction of sulfate production rates. Shown in Figure 2a is the maximum model-predicted potential sulfate, a term which is defined as the calculated SO_4 plus the available SO_2 that can be further converted to SO_4. This quantity represents an upper estimate of sulfate produced from the assumed sulfate emissions. The potential sulfate values are found to better match the observations, with a tendency toward overprediction. This suggests that the emissions are not underestimated and that the conversion rate of SO_2 to sulfate in the current model simulations after the postmonsoon season may be too low. This implies that sulfate production needs to be reexamined for the tropical Indian

Table 2. Summary of Monthly Biomass Emissions[a]

	Jan	Feb	Mar	Apr	May	Jun	Jul	Aug	Sep	Oct	Nov	Dec
South Asia + Myanmar BC	2.36	12.92	50.40	36.38	3.78	0.08	0.19	0.04	0.03	1.53	0.00	0.11
South Asia + Myanmar OC	17.32	95.11	382.55	275.87	20.25	0.59	1.42	0.31	0.22	7.45	0.01	0.72

[a]*Reddy and Boucher*'s [2004] climatological biomass burning emission (latitude 0–40°N, longitude 55–100°E); units: Gg/month.

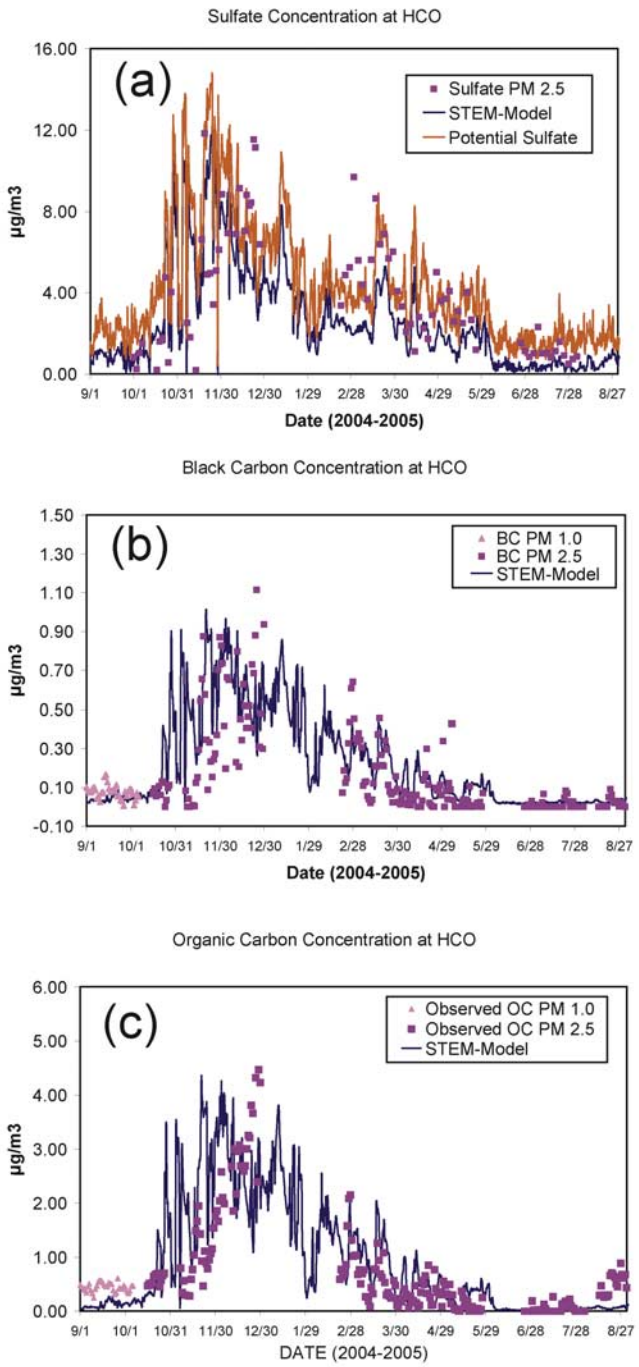

Figure 2. Model-predicted versus observed surface level sulfate (a), black carbon (BC) (b), and organic carbon (OC) (c) at Hanimaadhoo Climate Observatory (HCO).

subcontinent region, where abundant aerosol surface area is available for heterogeneous surface reactions, which may not be adequately represented in the current parameterization. Since there are no gaseous measurement of SO_2 available at HCO, SO_2 conversion rates could not be further constrained by observations.

[21] The comparison of observed BC (red squares) and modeled BC is shown in Figure 2b, and a similar comparison of OC is shown in Figure 2c. PM 1.0 μm size BC and OC measurements are available from September to October, and these are also shown in Figures 2b and 2c. The seasonal cycles of BC and OC are similar to those for sulfate. BC and OC show observed maximum values of approximately 1.1 and 4.5 $\mu g/m^3$, with background levels of approximately 0.1 and 0.4 $\mu g/m^3$, respectively. The model underpredicts observed BC and OC concentrations during the month of September. The observations show a rise in aerosol concentration from the middle of November while the model shows the rise from the end of October. The model is able to capture the peak concentration for BC and sulfate during November but underestimates the observed peak OC concentrations at the end of December. The model predicts the low concentrations of OC for June and July but fails to predict the rise in August as shown by observations.

[22] A notable feature in all the comparison is that the arrival of elevated polluted air masses in the predictions is approximately 20 d earlier than that observed. This will be discussed in more detail in section 3.3.

3.2. Seasonality of Aerosols at the Kathmandu Observatory

[23] Figures 3a–3c show the sulfate, BC, and OC observations and model predictions at the KTM site. Sulfate observations at KTM do not show as distinct a seasonality as seen at HCO. The observations show that the sulfate concentrations are around 2.0 $\mu g/m^3$ until January with a spike in late December when the values reach as high as 8.0 $\mu g/m^3$. The next set of observations start in early April and run through May 2005, with values of $\sim$3.0 $\mu g/m^3$. The model predictions for sulfate aerosol over KTM show elevated sulfate concentrations of around 10.0 $\mu g/m^3$ in September and declining to 1.0 $\mu g/m^3$ by mid-December. The model predicts the same low sulfate concentrations from mid-December to mid-March after which the modeled sulfate shows a steady rise and is comparable to the observations during the months of March to April 2005. The model predicts elevated levels of sulfate in KTM throughout the time period that ends on 31 August 2005. The elevated sulfate prediction during the monsoon and the postmonsoon season over KTM is explained by the dry model bias in predicting rainfall, which is discussed later in section 3.3.

[24] Figures 3b–3c illustrate the observed and modeled BC and OC over KTM. Observations of BC and OC do show a distinct seasonality over KTM site. Elevated levels of BC and OC are seen after the postmonsoonal months and the dry months extending up to May. The observations show higher BC and OC loading over the KTM site during the postdry transition than during the postmonsoon transition which is in contrast to the observations from the HCO site. Quantitatively, observations of BC at KTM show that BC concentrations are around 1.0 $\mu g/m^3$ from September until the middle of November when the concentrations rise and reach a value of $\sim$3.5 $\mu g/m^3$, while the observed OC concentrations show a rise from approximately 2.0 $\mu g/m^3$ to 16 $\mu g/m^3$ during the same time period. The next set of observations started in April 2005, and it shows fairly elevated levels of BC and OC with maximum values as high as 4 $\mu g/m^3$ and 51 $\mu g/m^3$, respectively. The last set of BC and OC measurements in KTM shown are during

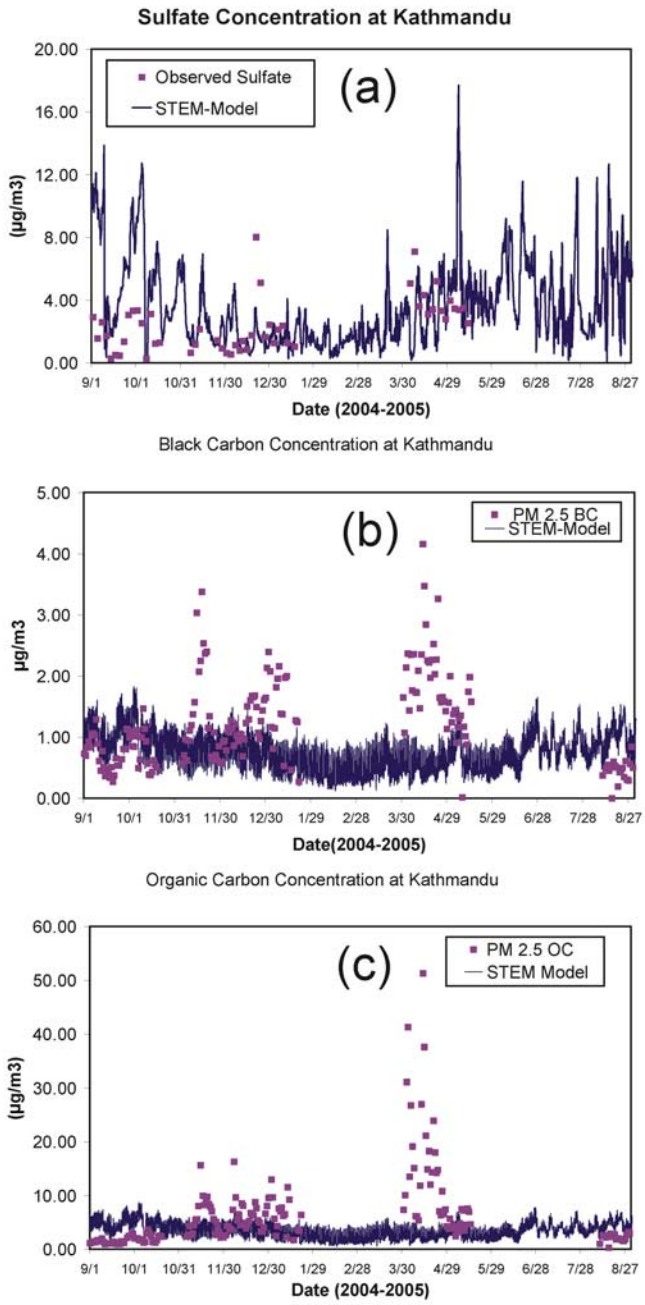

Figure 3. Model versus observed surface level sulfate (a), BC (b), and OC (c) at Kathmandu.

August 2005 with fairly constant and relatively low values of both BC and OC of about approximately 0.5 $\mu g/m^3$ and 3.0 $\mu g/m^3$, respectively. The model predictions show no seasonality in BC and OC concentration over KTM, but show a distinct diurnal variation of 0.75 $\mu g/m^3$ and 3.5 $\mu g/m^3$ BC and OC, respectively. Probable factors contributing to the seasonality of anthropogenic aerosol over KTM not presently included in this model calculations are discussed in section 3.4.

3.3. Seasonal Variation of Meteorological Conditions at HCO and KTM

[25] The seasonal variations in meteorological conditions play a large role in the seasonal aerosol cycles described in sections 3.1 and 3.2. A broad perspective to the seasonal transport patterns is seen in Figure 4 where the model-predicted surface layer winds over south Asia for the months of November, April, and July are shown. November represents the postmonsoon period, April represents the postdry transition, and July is representative of the summer monsoon. Five-day back-trajectory analysis of surface wind vectors (50 m) assist in identifying the pollutant source region for these characteristic months in bringing air masses to these two locations as shown in Figure 5. Here daily three-dimensional back-trajectories at HCO (Figure 5, top) and KTM (Figure 5, bottom) for the months of late November (15–30 November), April (1–15 April), and July (1–15 July) are shown. These trajectories are calculated using the MM5 winds and are initiated at a height of 50 m. Figure 5 shows that different air mass source locations affect these two observation sites during the three different months.

[26] Studying the monthly wind vectors from September 2004 to August 2005 (not shown), the modeled surface winds are calm and variable in direction in the highly populated Indian states of Bihar, Uttar Pradesh, and in some months extending west up to New Delhi and east to Kolkata. The surface winds over Nepal are usually variable in direction and slightly higher in magnitude than Bihar and Uttar Pradesh. These low wind speeds with variable wind direction contribute to high aerosol loading throughout the year. The winds are easterly over much of south India and the Arabian Sea in the month of November; therefore the windblown dust concentrations are low over the entire south Asia during this month since the dust emission source area is mainly the Middle Eastern countries. March–April is a high biomass burning season for south Asia and southeastern Asia. Since the winds are westerly over much of Myanmar during this month, the affect of southeastern biomass burning on aerosol concentrations over south Asia is minimal. The months of June, July, and August are monsoonal months over much of south Asia with strong southerly flows from the Arabian Sea and the Bay of Bengal.

[27] The seasonal variation in observed and predicted wind direction and speed at HCO is shown in Figure 6. This figure shows that October–November is a postmonsoonal transition period where the winds shift direction from westerly/southwesterly to easterly and northeasterly bringing polluted air mass from the Indian subcontinent and Southeast Asia. The 5-d back-trajectory of wind vectors from HCO shown in Figure 5a illustrates this postmonsoonal transition where the wind directions are variable and change rather abruptly. This helps explain the variability of the modeled BC and OC predictions at HCO during the postmonsoonal transition period depending upon which way the wind is blowing. Precise modeling of this transition remains a challenge for current meteorological models. For example, during the postmonsoon transition period (shown in Figure 6), the winds at HCO change direction from westerly/southwesterly to easterly and northeasterly. Then there is a gradual shift in the wind direction back to westerly

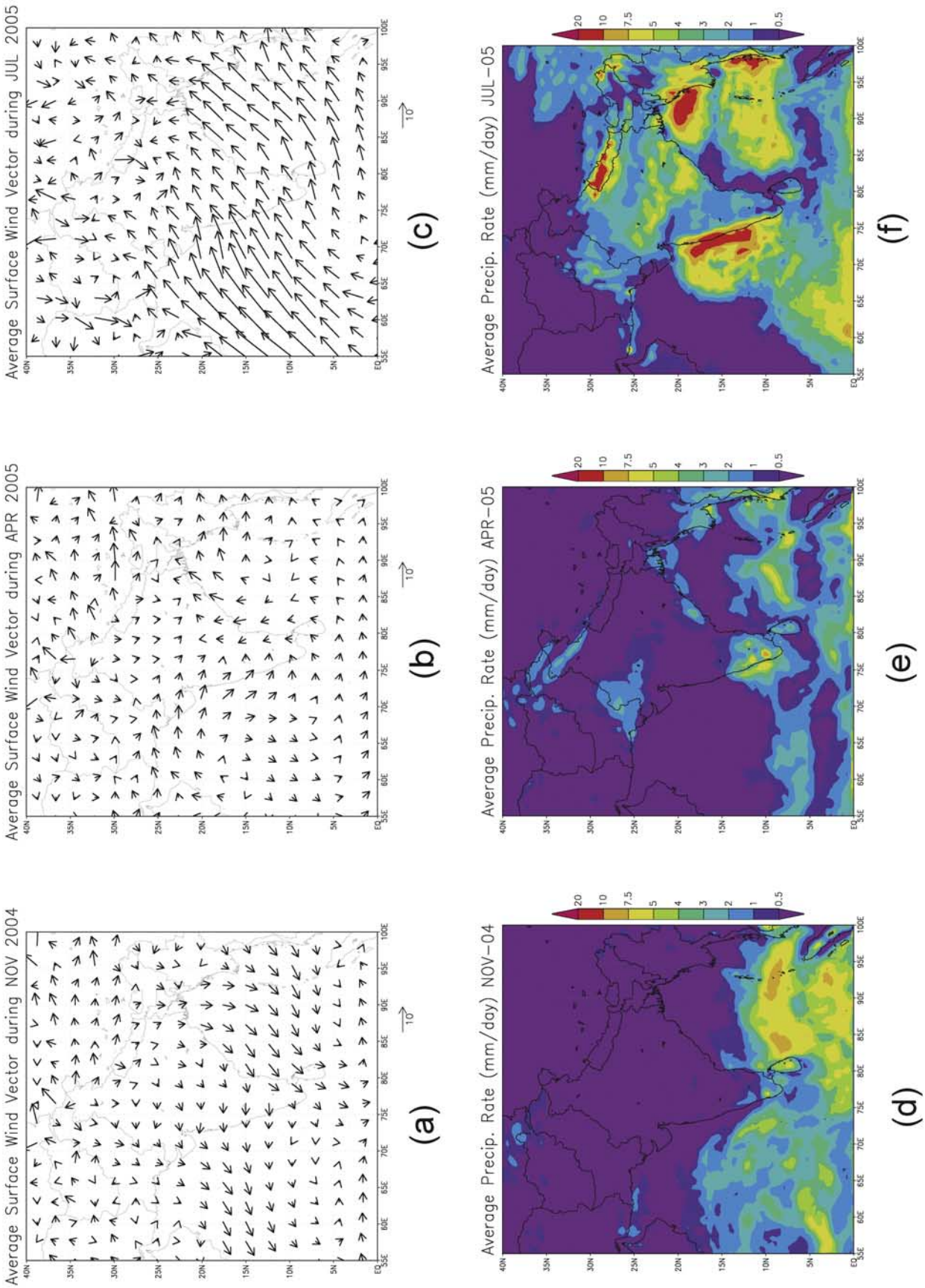

Figure 4. Model-calculated monthly averaged surface wind vectors during (a) November, (b) April, and (c) July and monthly averaged daily precipitation during (d) November, (e) April, and (f) July.

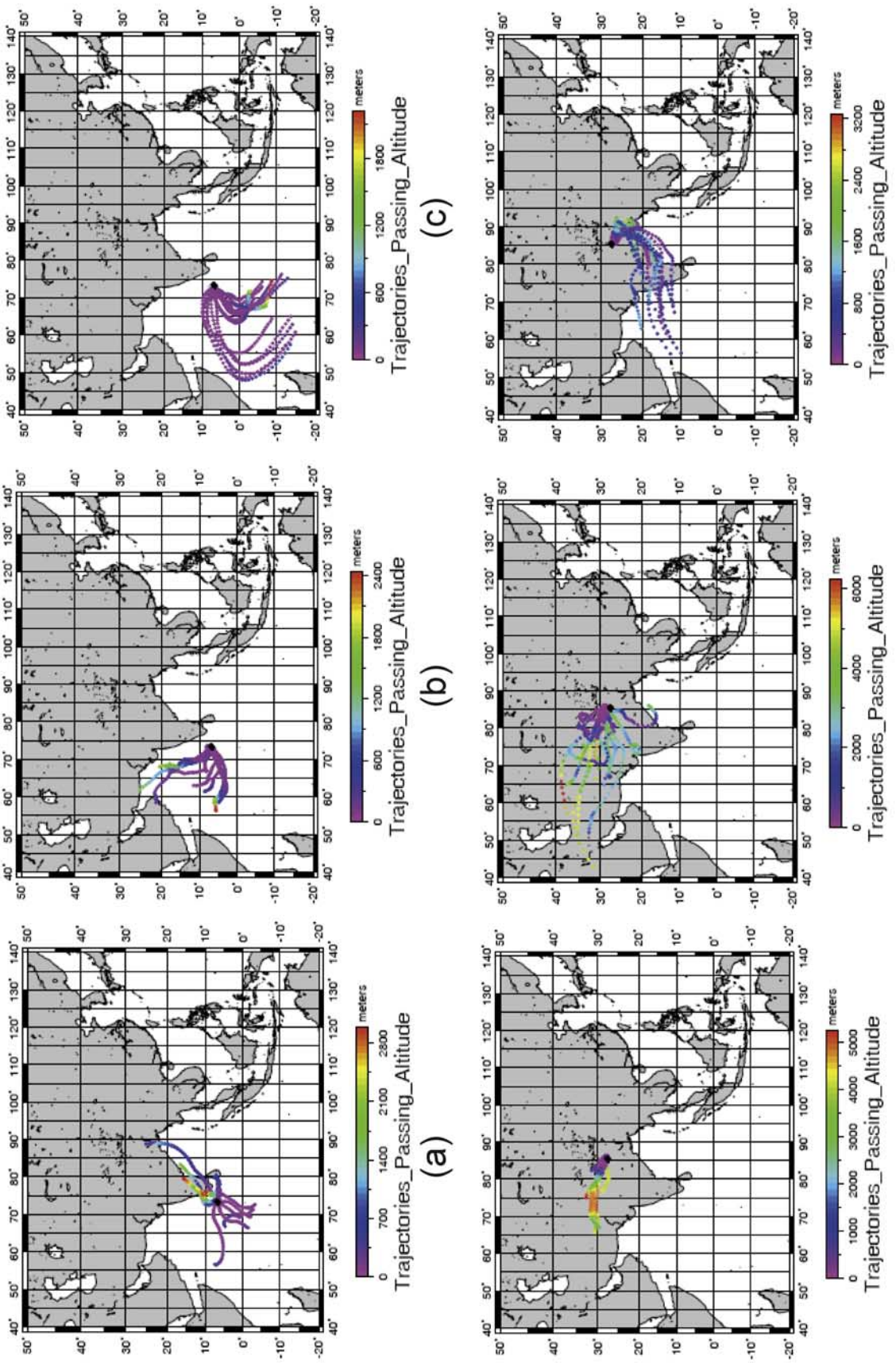

Figure 5. Three-dimensional 5-d back-trajectories arriving at HCO at 50 m during (a) November, (b) April, and (c) July and at Kathmandu Observatory (KTM) during (d) November, (e) April, and (f) July.

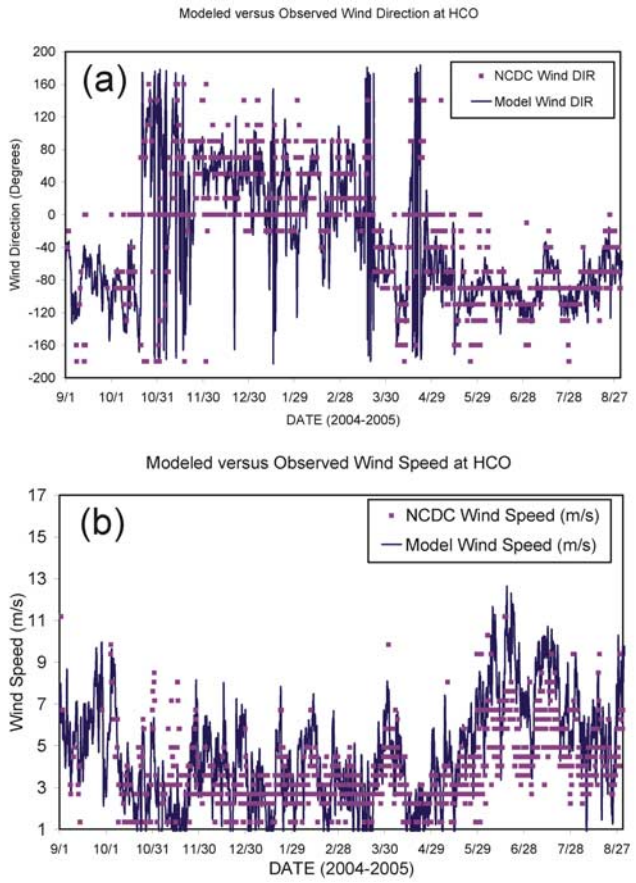

Figure 6. Model-predicted versus National Climatic Data Center (NCDC) provided observed wind direction (a) and wind speed (b) at HCO.

winds before the onset of the summer monsoon. Comparison of modeled wind direction and speed with observations from the National Climatic Data Center show that the model is able to capture the overall seasonal trend at HCO, although it misses one strong observed spike in wind speed in early November. Errors in wind speed during this transition period may help explain the difference in predicted aerosol concentrations which show high values while the observed show low values of BC and OC. The model captures the magnitude of the wind speed throughout the year except from mid-May to mid-July when the model predictions are higher than those observed.

[28] Monthly averaged model precipitation over south Asia is shown in Figures 4d–4f. Compared to the observed rainfall based on the Global Precipitation Climatology Project (GPCP) [*Huffman et al.*, 2001] (not shown), the simulated rainfall amounts are realistic over the Indian subcontinent and the nearby oceans from November 2004 through April 2005 with a slight dry bias. The model predictions of precipitation during the monsoonal months also generally show a slight dry bias. In July 2005, however, the anomalous rainfall observed in northeastern India is underpredicted by the model by up to 50%. Although November is a dry period over much of the Indian subcontinent, the Indian Ocean does see a significant amount of rainfall. Aerosols arriving at HCO during this period are subjected to wet scavenging. Since the model does have a dry bias, the model predicts higher aerosol concentration at HCO during this transition month.

[29] The 5-d back-trajectories arriving at KTM show that the air masses that come to KTM in April are also subjected to wet removal along their transport from the continent and thus are subject to wet scavenging. The month of July shows heavy precipitation all over the Indian subcontinent and the Bay of Bengal. The aerosols simulated at KTM are likely affected by the dry bias in northeastern India, since the back-trajectories in Figure 5f indicate frequent passage of air masses over northeastern India before arriving at KTM.

[30] Aerosol removal processes for BC and OC play an important role in the seasonality of the aerosol distribution and are a significant source of uncertainty in model predictions [*Bates et al.*, 2006]. The strong seasonality in precipitation patterns in south Asia introduces a strong seasonality in the wet removal of aerosols. Seasonal changes in wind speed impact the dry seasonal deposition of particles. To study the model sensitivity to these factors, additional simulations were performed. To study the sensitivity of the model to dry deposition, a simulation was conducted with the dry deposition velocity increased by a factor of 10. A second sensitivity study was carried out to examine the effect of the wet scavenging parameter for carbonaceous aerosol. As mentioned previously, BC and OC are modeled as hydrophobic and hydrophilic aerosols. Only the hydrophilic BC and OC aerosols are subject to wet scavenging by precipitation. Sensitivity simulations were performed with BC-OC precipitation scavenging efficiency the same as the removal efficiency of sulfate aerosol, and with removal efficiency equal to 10% of the sulfate aerosol removal efficiency.

[31] Analyzing the changes in model-calculated BC concentrations from these sensitivity simulations for HCO, it is observed that during the dry season (as expected), dry deposition velocity has a large impact on calculated concentrations of BC. These results are shown in Figure 7a. However, during the postmonsoonal transition period wet deposition plays an important role. The maximum percentage change in BC concentration is approximately 100% and 168% for changes in dry deposition velocity and wet scavenging efficiency at HCO. As discussed earlier, the predicted aerosol values are higher than observed during the postmonsoonal transition month of November. These results suggest that the removal processes may be too low in the model. This is an area that requires further study. Similar sensitivity results are found for KTM and are shown in Figure 7b. The maximum percentage change in BC concentration is approximately 63% and 65% for changes in dry deposition velocity and wet scavenging efficiency at KTM, respectively.

3.4. Emissions as a Contributor to the Seasonal Cycle

[32] The seasonal variation in emissions is another important factor that influences the seasonal cycle of aerosol distributions in south Asia. As discussed previously in section 3.4, open biomass burning has an important seasonal cycle that contributes to the seasonality of BC and OC loadings over south Asia. Other important sources also have

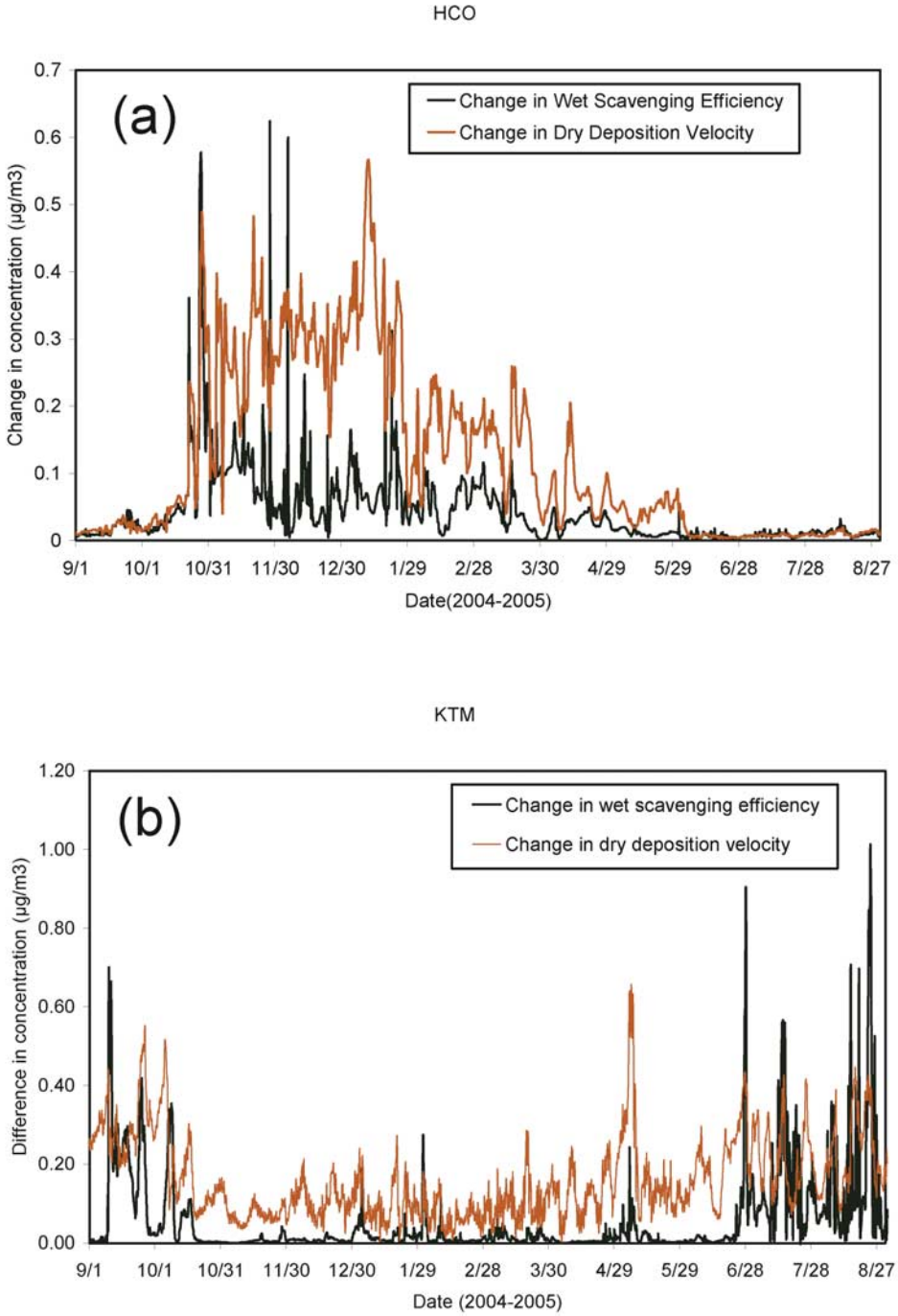

Figure 7. Absolute difference in BC concentration between different model sensitivity studies at (a) HCO and (b) KTM.

seasonal emissions. For example, the Kathmandu valley has approximately 125 brick kilns that operate only in the dry months of December to April. These brick kilns are rather crude technologically, and the business practice is to use the cheapest kind of coal and other biofuels available at the time for combustion. The Nepal Ministry of Environment and Population together with Environmental Sector Program Support (a Danish Government and Government of Nepal project) performed an emissions inventory of brick kilns operating in Nepal for the year 2001. They estimate the emissions of SO_2 to be 4.32 G tons/a which is almost the same amount for the total annual area emission sources in the Trace-P inventory (4.02 G tons/a for that grid cell). Preliminary simulations for SO_2 using the kiln emission estimates show that the predicted SO_2 levels at the KTM site increase approximately by a factor of 3–4. The kiln study did not provide any estimate of BC and OC emissions from the brick kilns. *Reddy and Venkataraman* [2002] report that the BC and OC emissions from coal combustion in the brick kilns in India are an order of magnitude higher

than controlled combustion in the power plants and industries. Increases in BC and OC emissions during brick kiln operation in Kathmandu valley could probably explain higher peak loadings during the dry months. Five-day back-trajectory analysis, discussed previously, showed that the winds are westerly during the high-OC and high-BC periods and originate from the northwestern states of India. Therefore the seasonality of emissions from this region also needs to be examined in more detail.

[33] The comparison of the observations with the model predictions during this study period provide some insights into the quality of the emission estimates used in the analysis. The comparison of BC, sulfate, and OC values at HCO suggest that the regional emissions of these species (and precursors) are qualitatively correct. Valuable information regarding the emissions is also contained in the ratio of aerosol species. A comparison of BC to sulfate aerosol fine-mode ratios (based on concentration) observed and predicted at Kathmandu and HCO is shown in Figures 8b–8c. As shown, the ratios demonstrate a seasonal cycle that is also captured by the predictions (even for Kathmandu). These seasonal variations reflect the contributions from different source regions. The BC to SO_2 ratio for the emissions is also shown, and the high values over land reflect those regions with large emissions from biofuels and/or biomass open burning. The elevated values over the oceans reflect contributions from ship emissions. At HCO the BC to sulfate ratio increases as the air masses from south India reach the measurement site. At Kathmandu the ratio increases for periods when the flow is from the south and east and the ratio values do show seasonality. The observed BC to OC ratios reach maximum value at HCO during the high-aerosol periods with values $\sim$0.5. At Kathmandu the highest values are in September with values reaching $\sim$0.9; the ratios vary between 0.1 and 0.3 during the dry season. The model predictions (not shown) are able to reflect the variability of the BC to OC ratio at HCO, but show almost no variability at Kathmandu.

[34] Further insights into seasonal transport and source contributions to aerosol distributions can be derived by model simulation using regionally tagged CO tracers (as described by *Uno et al.* [2003b]). The main purpose of a chemical tracer model is to identify major features with the outflow of pollutants from a defined geographic region. Therefore all initial conditions and inflow boundary conditions of CO are set to zero. *Uno et al.* [2003b] used this technique to help identify air masses from different sources during the Trace-P, ACE-Asia, and ITCT-2K2 field experiments. The results from this study illustrating the contribution of polluted air mass over HCO from India, Sri Lanka, and Southeast Asia (up to 110°E longitude) for the dry months starting 1 October 2004 to 1 February 2005 are shown in Figures 9a–9b for the surface layer and the 3500 m layer. The results show that at the surface layer the contribution is largest from south India, followed by north India and Southeast Asia. The contribution from Sri Lanka is less than 10%. However, the largest contribution to polluted air mass over HCO at the 3500 m layer is dominated by Southeast Asia. The wind vectors at this layer are higher in wind speed, and the directions are easterly compared to surface layer where the winds are northeasterly. The contributions from north India and Sri Lanka remain similar.

[35] Similar analysis was performed using biomass and fossil fuel (including biofuel) tracers. Model calculations at the surface show that the average contribution of biomass burning to total (fossil fuel + biomass) is $\sim$34% for the months of 1 October 2004 to 1 February 2005 with values ranging from 10–60%. At the elevated layer (3500 m) the contribution of biomass increases slightly with average being equal to $\sim$45%; the individual day values range from 15% to 75%.

[36] Finally, windblown dust is another source term with a pronounced seasonal cycle. South Asian dust show a distinct seasonality with peak loadings during the late dry period to early monsoon season. Dust emissions are very uncertain; they vary from model to model by a factor of 3–5 [*Bates et al.*, 2006; *Uno et al.*, 2004]. In this study we applied a dust emission parameterization that we have used successfully for east Asia [*Tang et al.*, 2004; *Uno et al.*, 2004]. We found that our dust mass concentrations when compared to the ABC observations of $PM_{2.5}$ and PM_{10} accurately captured the day to day variability but were too high. Thus we adjusted our dust calculation algorithm and decreased the dust emission coefficient by a fraction of 3.25 for applications over south Asia. Figures 10a and 10b show the comparison of fine-mode STEM-predicted $PM_{2.5}$ mass with $PM_{2.5}$ observations at HCO and KTM after adjusting the dust emissions. Figure 10a shows good agreement with total $PM_{2.5}$ observations at HCO, while the $PM_{2.5}$ predictions are still slightly higher over KTM. The PM_{10}-predicted mass (not shown) also agrees well with observed PM_{10} mass at HCO and captures the seasonality and magnitude, but in the dry months of November to March it underpredicts the observed PM_{10} mass.

3.5. Aerosol Distribution and Composition Over South Asia

[37] Chemical transport models provide a means to place the ABC observations into a regional context. The predicted regional surface distributions of sulfate, BC, and OC over south Asia for the postmonsoon (November), postdry (April), and the monsoon (July) periods are presented in Figures 11a–11i. In general, much of south Asia has high concentrations of sulfate in the postmonsoon season, while during the postdry transition period the concentrations are reduced but with concentrations remaining elevated over the Ganges valley and Bangladesh. The summer monsoon cleans out southern India and the eastern part of the Ganges valley while pollution starts to build up over the northwestern part. The predictions show that despite heavy rainfall from the monsoon in July, the precipitation is not able to completely cleanse the environment over the Ganges valley. Although our model has a dry bias, experimental observation of aerosol optical depth at Kanpur (discussed in section 3.6) also corroborates this result. During the postdry transition, elevated BC and OC concentration over south India as seen in Figures 11e and 11h are due to biomass burning. Myanmar sees a stronger rise in BC and OC concentration because of biomass burning over the region during this time.

[38] During the postmonsoon period the outflow of aerosol from south Asia to the Indian Ocean and the Bay of Bengal is significant. Most areas of the Arabian Sea and the Bay of Bengal see elevated sulfate concentrations of more

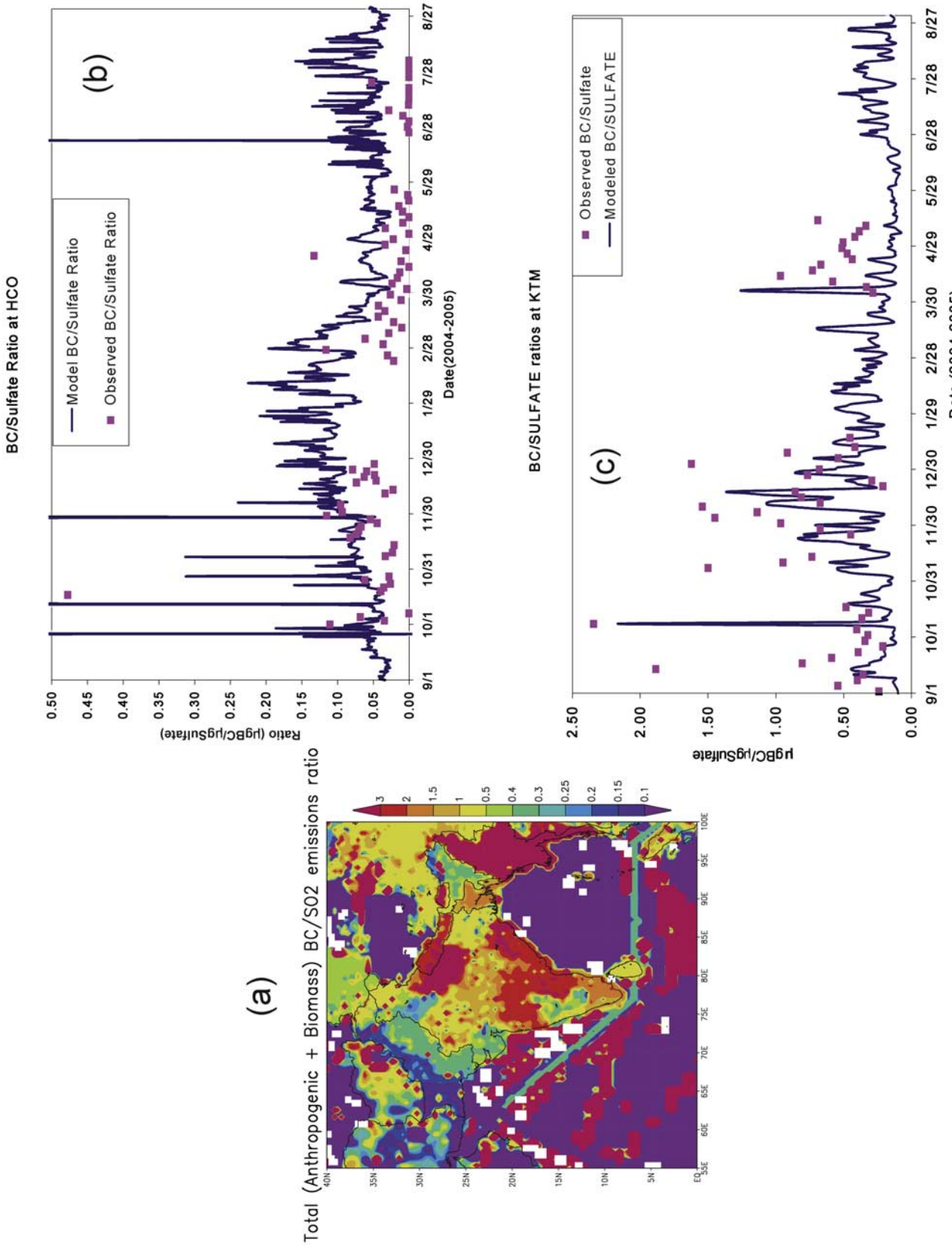

Figure 8. (a) Ratio of BC to SO_2 emissions used as model input with ratios of observed and model-predicted BC to sulfate concentrations at (b) HCO and (c) KTM.

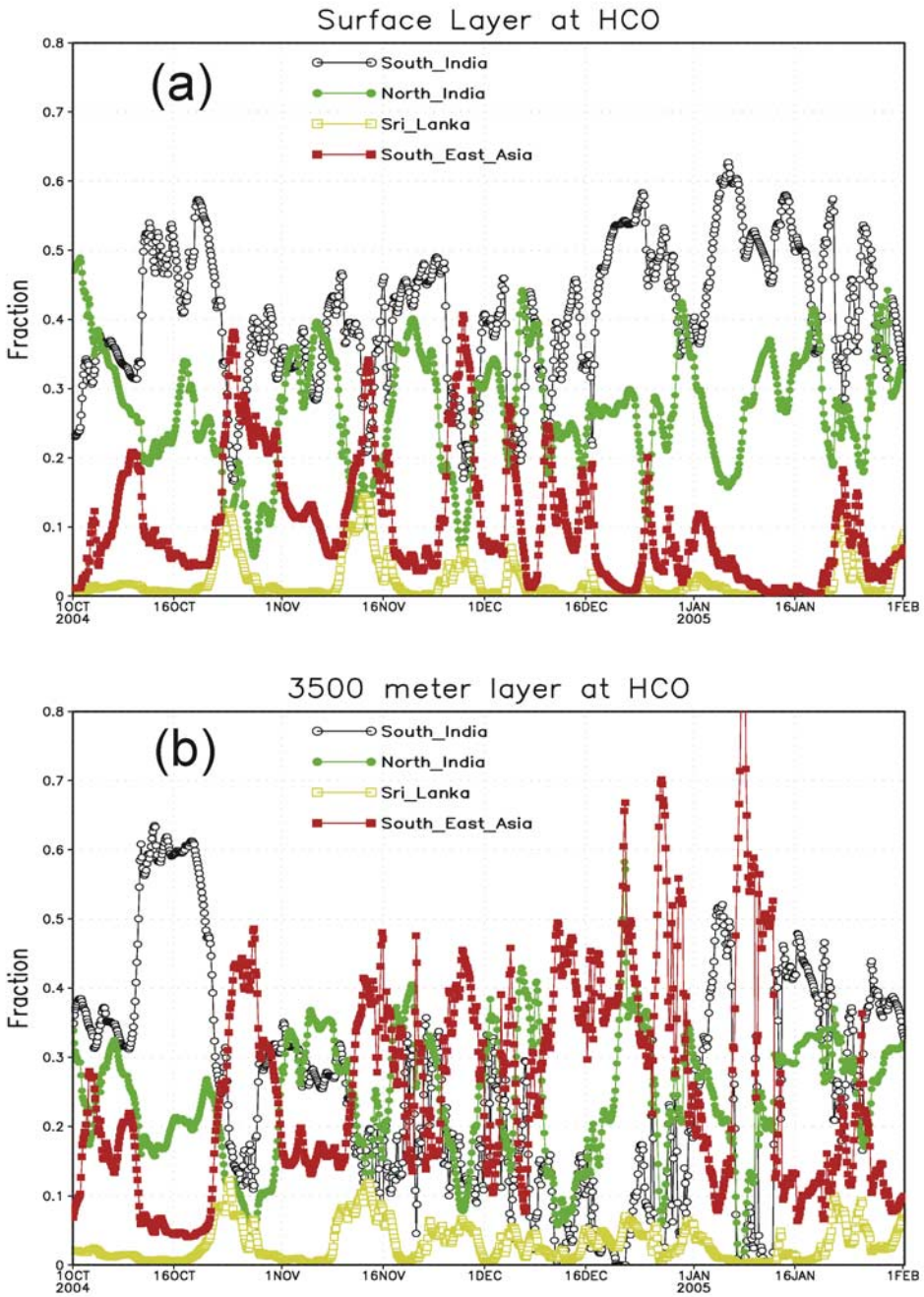

Figure 9. Geographical region tagged air mass tracers that show the fractional contribution to polluted air over HCO at the (a) surface layer and (b) 3500 m layer.

than 10 $\mu g/m^3$, of 0.7 $\mu g/m^3$ of BC, and of 3 $\mu g/m^3$ of OC. During the postdry transition period the northernmost portion of the Bay of Bengal still experiences elevated levels of aerosols, while the aerosol levels over the Arabian Sea decline to background levels. During the monsoonal months the aerosol levels in the Arabian Sea are at background levels, while over the Bay of Bengal there are still elevated levels of aerosol. This is because monsoonal winds transport polluted air masses from south India into the Bay of Bengal. The wind flow is easier to visualize from the back-trajectory results at KTM presented earlier in Figure 5f.

[39] To further illustrate the seasonal variation of aerosols in south Asia, the predicted monthly averaged aerosol composition in model grid cells that contain five cites in south Asia were analyzed (see Figure 12). The two cities KTM and HCO are chosen as we have observations to constrain the model, and they are also end points of the modeling domain with very different emissions and meteorological conditions. The three other cities, Kanpur (latitude 26.44°N, longitude 80.34°E), Pune (latitude 18.53°N, longitude 73.85°E), and Bangalore (latitude 12.96°N, longitude 77.58°E), were chosen such that they

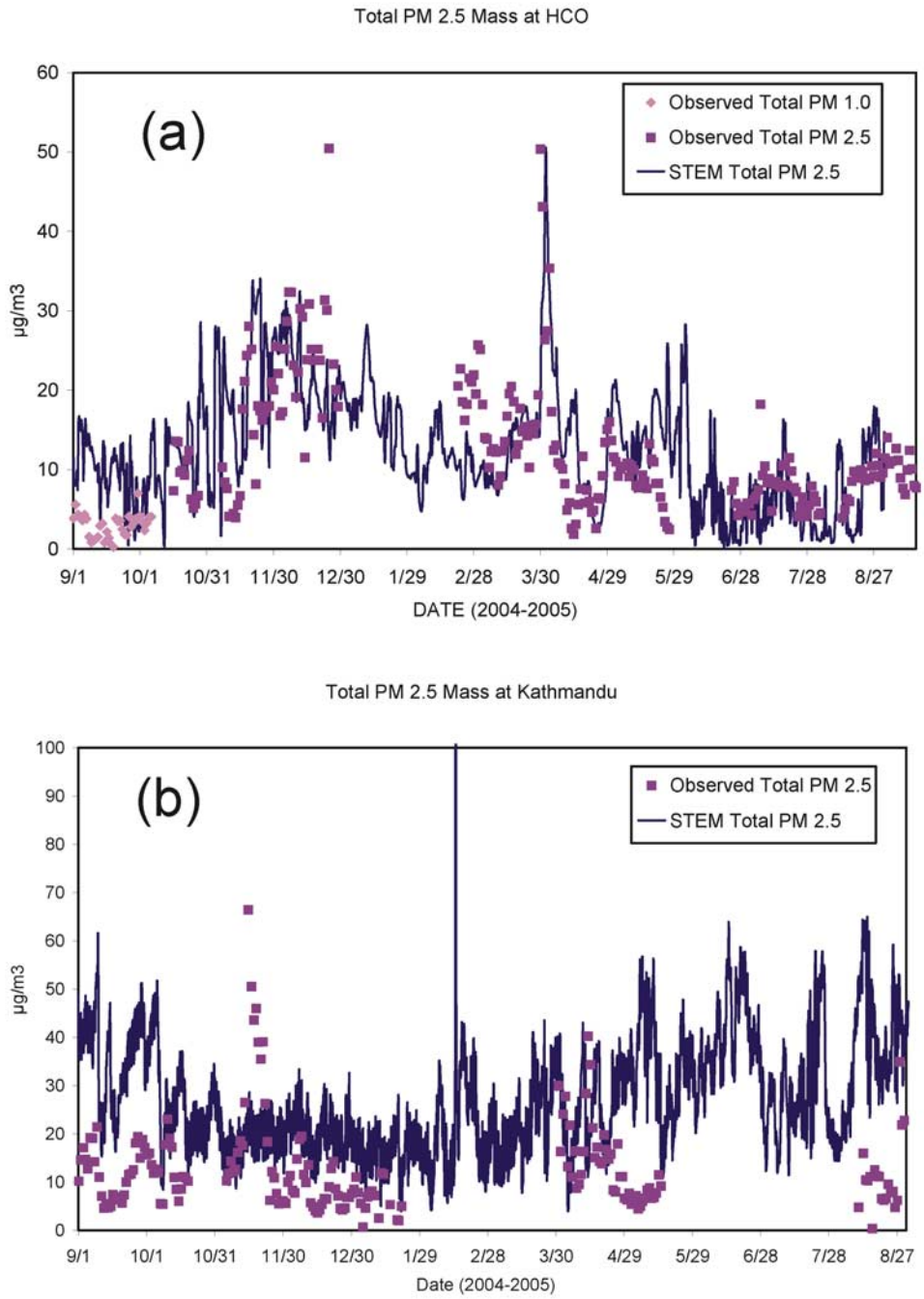

Figure 10. Model versus observed PM mass at (a) HCO and (b) Kathmandu.

represent different spatial locations as well as different emissions and meteorological conditions.

[40] The fine-mode aerosol concentration at these locations is presented in Figure 12. While the sulfate, BC, OC, and other $PM_{2.5}$ have been discussed separately (see Figures 2–3 and Figure 10), here we show the combined aerosol composition. Of particular importance is the contribution of anthropogenic aerosols to the fine mode. The postmonsoonal months and the early dry season show high-anthropogenic aerosol loading, with significant amounts of other emitted $PM_{2.5}$ aerosol as well as sulfate. The postdry transition months of March–May see a decline in anthropogenic aerosols. The monsoonal months show that the fine-mode aerosol is mainly windblown dust.

[41] The seasonal cycle of fine-mode aerosol at KTM differs from the other sites. Furthermore the carbonaceous aerosols exceed sulfate aerosol levels throughout the year at KTM. At Kanpur, other emitted $PM_{2.5}$ aerosol is the dominant fine-mode aerosol throughout much of the year. Fine-mode dust is significant in the aerosol composition in

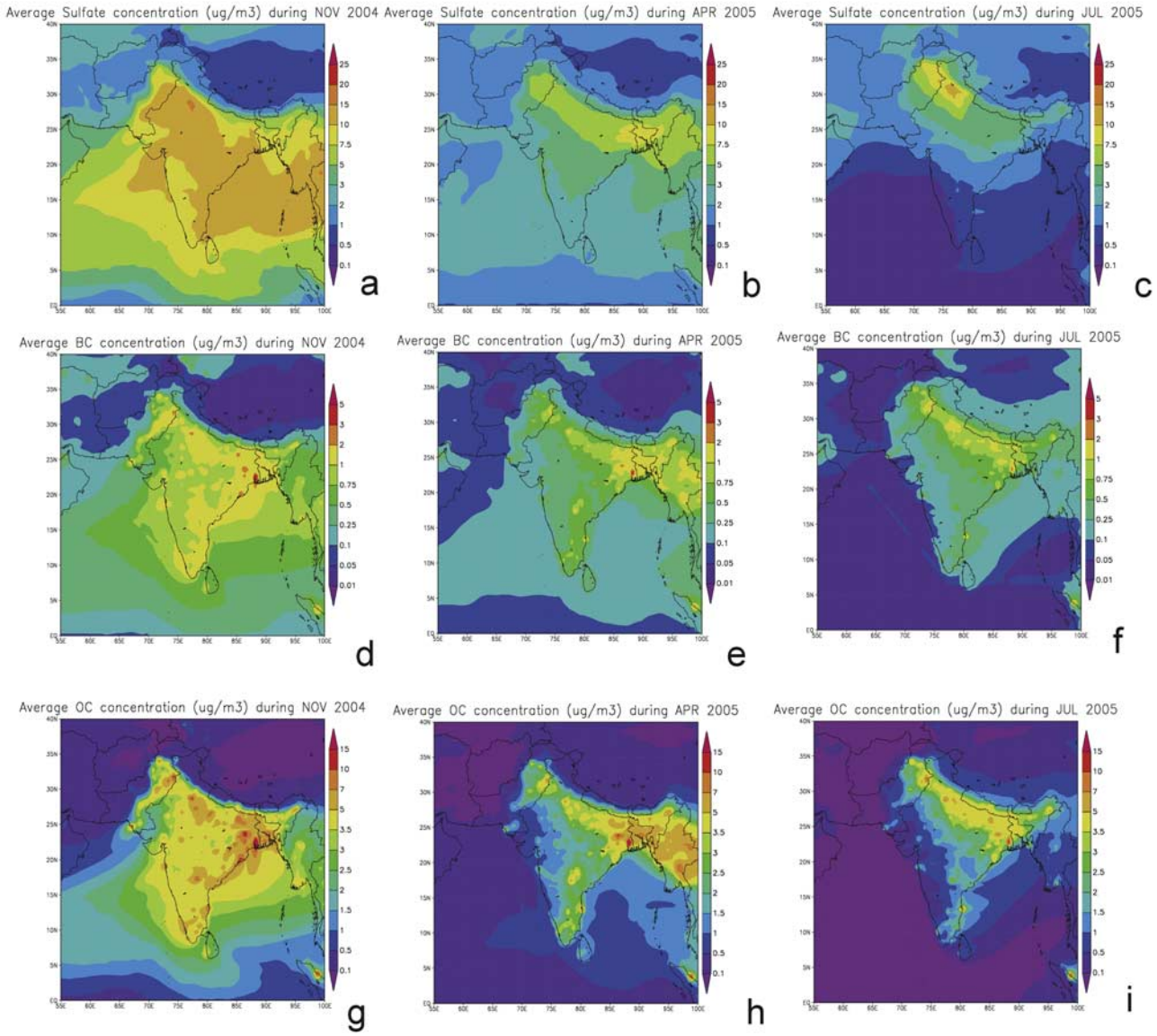

Figure 11. Predicted surface level monthly average sulfate concentrations during (a) November, (b) April, and (c) July, average black carbon concentrations during (d) November, (e) April, and (f) July, and organic carbon concentration during (g) November, (h) April, and (i) July.

the postdry transition and monsoonal months. The contribution of carbonaceous aerosol is as high as sulfate aerosol after the postmonsoon transition period. Although Kanpur is closer to KTM, it shows peak anthropogenic aerosol concentration in the postmonsoonal period and declining values thereafter (as seen over HCO). This pattern is unlike KTM where the peak anthropogenic aerosol distribution is seen in late monsoon with lowest anthropogenic aerosol concentration in the dry period.

[42] The fine-mode aerosol composition at Pune, shown in Figure 12d, illustrates a different aerosol monthly distribution and composition than the previously discussed three cities. Dust is dominant throughout the year except during the postmonsoon transition period where anthropogenic aerosols dominate. Fine-mode sea salt is also seen in the monsoonal months at Pune.

[43] At Bangalore the anthropogenic aerosols dominate the fine-mode aerosol composition from the postmonsoon up to the end of the dry period. The other (non-BC and non-OC) emitted $PM_{2.5}$ emissions dominate over sulfate, OC, and BC. The peak concentration is seen in November and gradually declines throughout the year. The fine-mode anthropogenic aerosol composition over Bangalore shows similar seasonality as HCO.

[44] The coarse-mode aerosols at these five sites are shown in Figure 13. Windblown dust and anthropogenic other PM_{10} dominate the coarse mode at all sites and all seasons. Significant amounts of coarse sea salts are seen only in June and July transported inland with the monsoon. The coarse-mode dust loading in south Asia increases significantly after the late dry season until the end of the monsoon season when the winds reverse direction.

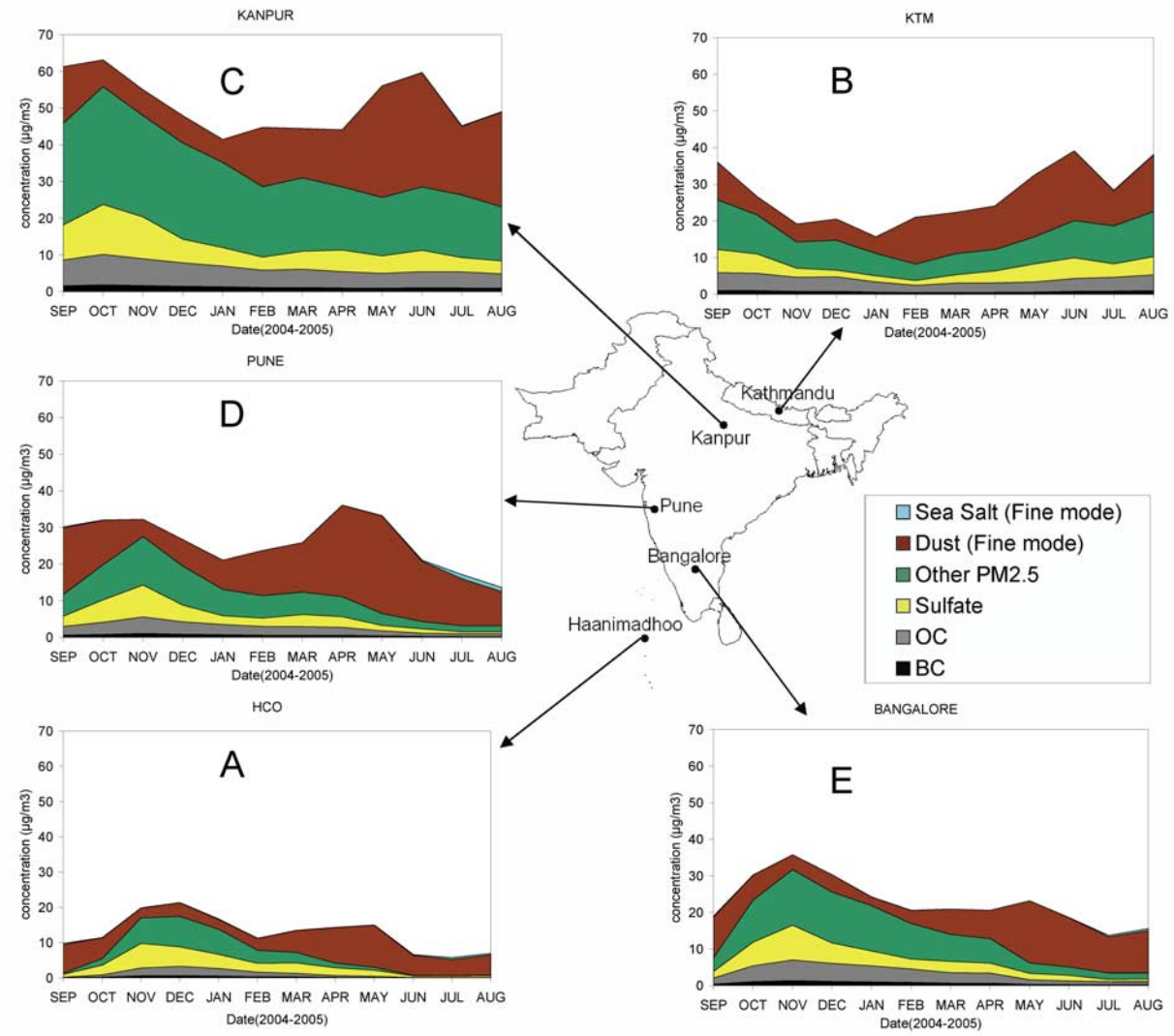

Figure 12. Model-calculated fine-mode chemical composition at (a) HCO, (b) KTM, (c) Kanpur, (d) Pune, and (e) Bangalore.

3.6. Aerosol Contribution to AOD

[45] The predicted three-dimensional aerosol distributions were used to predict aerosol optical depth (AOD). The AOD module of the STEM model calculates the aerosol optical depth using calculated aerosol concentration amount and aerosol species-specific extinction coefficient. The extinction coefficient parameters used in the calculations are reported in the paper by *Penner et al.* [2001]. In this section we focus on the spatial AOD distribution over south Asia and the city locations discussed in section 3.5. Since aerosol optical depth is the attenuation of solar radiation through the vertical column of the atmosphere, species contribution to AOD over south Asia differs from the surface aerosol composition. We first discuss the experimental AOD observations as further constraints for model predictions and then provide some insight into the species contribution to the total aerosol optical depth.

[46] Kanpur is the only AERONET site over south Asia that has at least a yearlong observation of aerosol optical depth during our simulation period. AERONET observations (Figure 14) of AOD over Kanpur show seasonality with high values in the postmonsoon and postdry transitions and low values in the middle of the dry season (February and March). This is consistent with the STEM model-predicted surface aerosol mass loadings over Kanpur. Figure 14 compares the STEM model total AOD (at 550 nm) with the AERONET observations (500 nm). The calculated AOD captures the seasonal trend of the observed AOD over Kanpur. During the postmonsoon period and the early dry season the model underestimates the observed AOD (by ~33%), but performs well during the other seasons. AERONET observation shows elevated aerosol optical depth during the monsoonal months of June, July, and August compared to the dry months of February and March. This observation confirms the model-predicted elevated aerosol loading over the Ganges valley during the monsoonal months.

[47] Figure 15a shows a comparison with the MICROTOPS AOD measured at HCO. The model results show

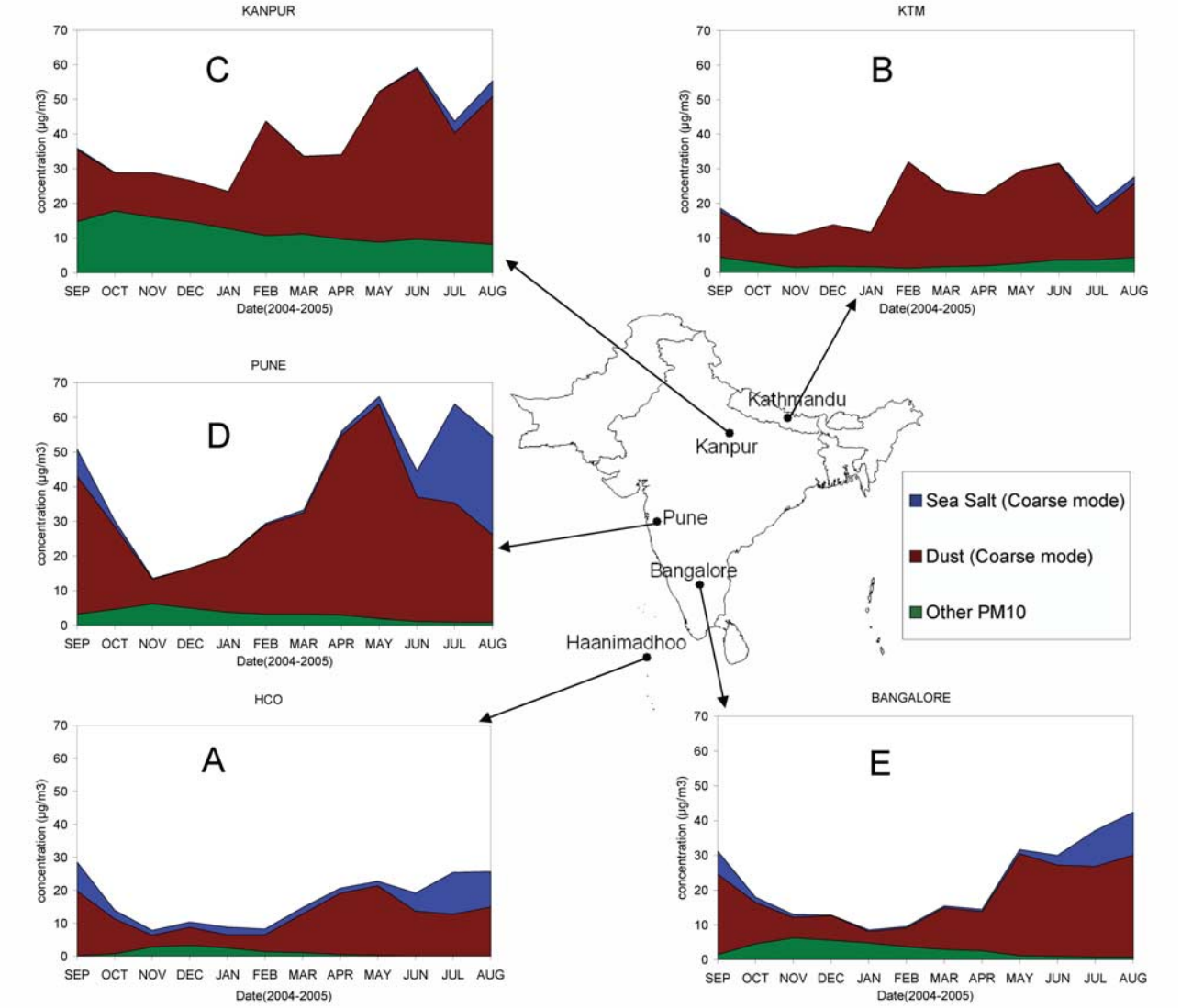

Figure 13. Model-calculated coarse-mode chemical composition at (a) HCO, (b) KTM, (c) Kanpur, (d) Pune, and (e) Bangalore.

good seasonal agreement with the observations from the dry period to mid-monsoon-season (mid-July). The overprediction of AOD afterward is due to an overprediction of dust. These results suggest that the model transports dust too far south, due in part to the MM5 precipitation bias discussed previously. Figure 15b shows the comparison of the Ångstrom exponent, which is a qualitative indicator of aerosol size, along with the calculated $PM_{2.5}$ to PM_{10} ratio. The synoptic variation in the predicted fine to coarse ratio is very consistent with that observed in the Ångstrom exponent data. These results show that coarse-mode aerosols increased during the monsoon period. The results show the maximum contribution of the anthropogenic aerosol (fine mode) occurs until the end of April.

[48] The calculated species contribution to the AOD at Kanpur and HCO are shown in Figures 16a and 16b. The total fine-mode contribution to AOD is also shown. The results show that the fine-mode contribution to total AOD is greater than 83% in the postmonsoon and the dry season at all of the five cities. At Kanpur, sulfate, BC, and OC fine-mode anthropogenic aerosol dominate the AOD from late monsoon to early dry season (with sulfate the largest single contributor), after which the contributions of dust increase. The contribution of windblown dust is maximal in the late dry season (May and June). The annual average contribution of absorbing aerosol to anthropogenic aerosol AOD over Kanpur is 15% with values ranging from 13 to 18%. At HCO the annual average contribution of absorbing aerosol to anthropogenic aerosol AOD over HCO is 5.8% with values ranging from 3.8 to 8.4%.

[49] Results for the other cites are also presented. Figure 16c shows the monthly averaged aerosol contribution to total AOD over KTM. Again, fine-mode dust and sulfate are significant contributors to total calculated AOD.

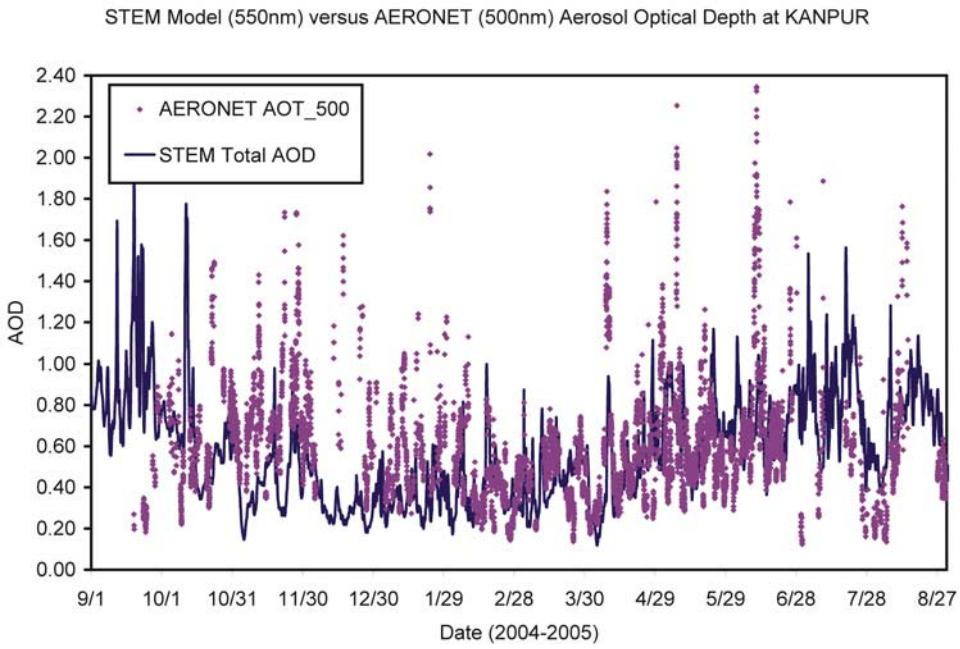

Figure 14. Model versus AERONET aerosol optical depth at Kanpur.

The AOD peaks in August with a value of 0.67. The dry months see a low aerosol optical depth, with the contributions from carbonaceous aerosol increasing in importance. It needs to be mentioned again that although the model overpredicts the total $PM_{2.5}$ mass at KTM, it misses the BC and OC peaks in the dry months; thus their contributions are underestimated. The modeled annual average contribution of absorbing aerosol to anthropogenic aerosol AOD over KTM is 16% with values ranging from 12 to 22%.

[50] At Pune, sulfate aerosol dominates the contribution to total AOD in the postmonsoon months. The lowest total AOD is shown for the dry months of December to March, where the AOD is dominated by anthropogenic aerosol and with the largest contributions from carbonaceous aerosols. This shift in anthropogenic aerosol composition reflects the impact of different source regions. Coarse- and fine-mode dust contribution to total AOD is highest in the late dry season. Coarse sea salt contribution to total AOD is high in the monsoonal months. The annual average contribution of absorbing aerosol to anthropogenic aerosol AOD over Pune is 13% with values ranging from 8 to 18%.

[51] Finally, the monthly averaged aerosol contribution to total AOD over Bangalore shows that AOD values peak at October, and the lowest values are found in February. The anthropogenic aerosols led by sulfate contribute significantly through the end of the dry season after which fine-mode dust contribution dominates. Unlike in Pune, the coarse-mode dust does not contribute significantly to AOD over Bangalore. During the monsoonal months the contribution of coarse sea salt and coarse dust contribution to AOD are similar. The annual average contribution of absorbing aerosol to anthropogenic aerosol AOD over HCO is 13% with values ranging from 9 to 19%.

[52] The annual average AOD, the contribution of anthropogenic aerosol to AOD, and the absorbing aerosol fraction over south Asia are shown in Figures 17a–17c. The STEM model results show anthropogenic AOD greater than 0.3 throughout the Ganges Valley with absorbing aerosols accounting for greater than 10% of the anthropogenic AOD throughout the Indian subcontinent. These values were used to quantify the ''Atmospheric Brown Cloud'' hotspots throughout the world using the GOCART chemical transport model and satellite based observations [*Ramanathan et al.*, 2007]. The Ramanathan et al. study points out strong seasonal dependence of atmospheric brown clouds throughout the world with five regional hotspots: east Asia (eastern China, Thailand, Vietnam, and Cambodia), Indo-Gangetic plains (from Pakistan across India to Myanmar), the Indonesian region, the southern region of sub-Saharan Africa, and the Amazon basin in South America. This STEM model study focused on South Asia is consistent with the satellite data assimilated GOCART model study in predicting the Indo-Gangetic region as one of the brown cloud hotspots. The Ramanathan et al. study also identifies 13 megacities (out of 26 total megacities) of the world influenced by atmospheric brown clouds; the megacities identified in South Asia are New Delhi, Karachi, Mumbai, Kolkata, and Dhaka. Their study points out that megacities in developed nations such as Tokyo, New York, and London have annual AOD exceeding 0.2, and megacities in South America have the lowest annual AOD. The STEM model result in Figure 17a shows that average annual AOD for these south Asian megacities are greater than 0.4 and are consistent with the study of Ramanathan et al.

4. Uncertainties and Future Work

[53] Modeling results indicate that more work is needed to improve the aerosol and precursor emissions in this region. For Kathmandu the seasonality of Brick Kiln emissions needs to be further examined and included in

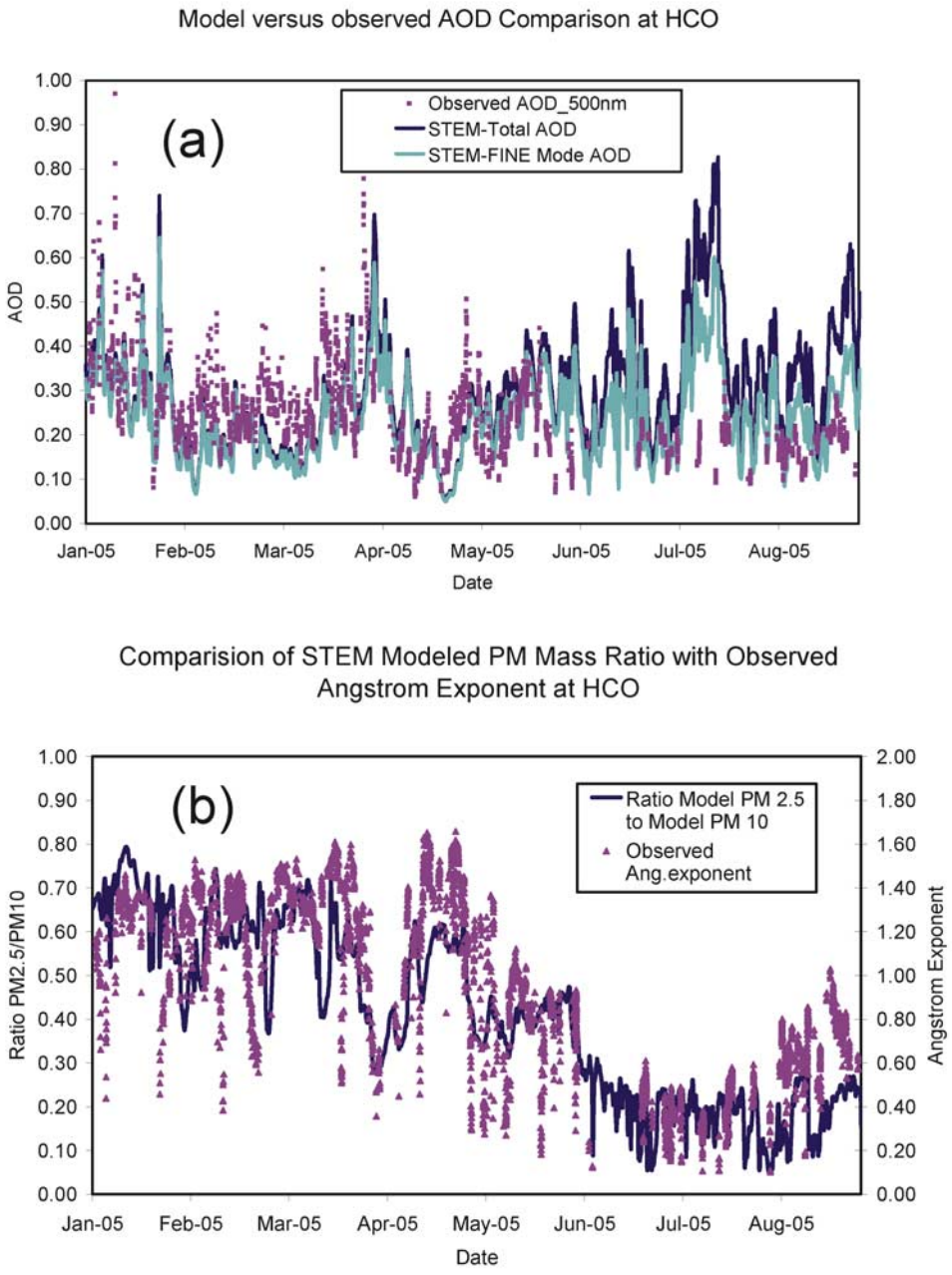

Figure 15. (a) Model versus observed aerosol optical depth and (b) PM mass ratio versus Ångstrom exponent comparison at HCO.

the analysis. In addition, the assessment of the impact of these kiln emissions on the KTM observation site will require a finer resolution modeling analysis. There is also a keen need to update the emission estimates of aerosols and precursors to reflect the 2004/2005 period, as current emission estimates are based on base information reflective of the circa 2000. The study was completed using climatological biomass burning inventory with a horizontal resolution of 1 × 1 degree; real-time emissions from biomass burning based on satellite fire counts on a finer grid resolution should improve model predictions. Much of this region is undergoing rapid economic growth with increases in energy use and emissions.

[54] However, emissions are not the only sources of uncertainty; sensitivity study with SO_2 conversion rates suggests that the model needs to reexamine the conversion rate during the dry period. Sensitivity studies on the dry deposition velocity of BC and wet scavenging efficiency for BC suggests that these model parameters need to be more thoroughly examined. Despite a higher-resolution meteorological modeling constrained by observations, the MM5 model needs improvement in predicting the precipitation amount.

[55] The chemical transport model is constrained only by observations at the surface, because of the lack of readily

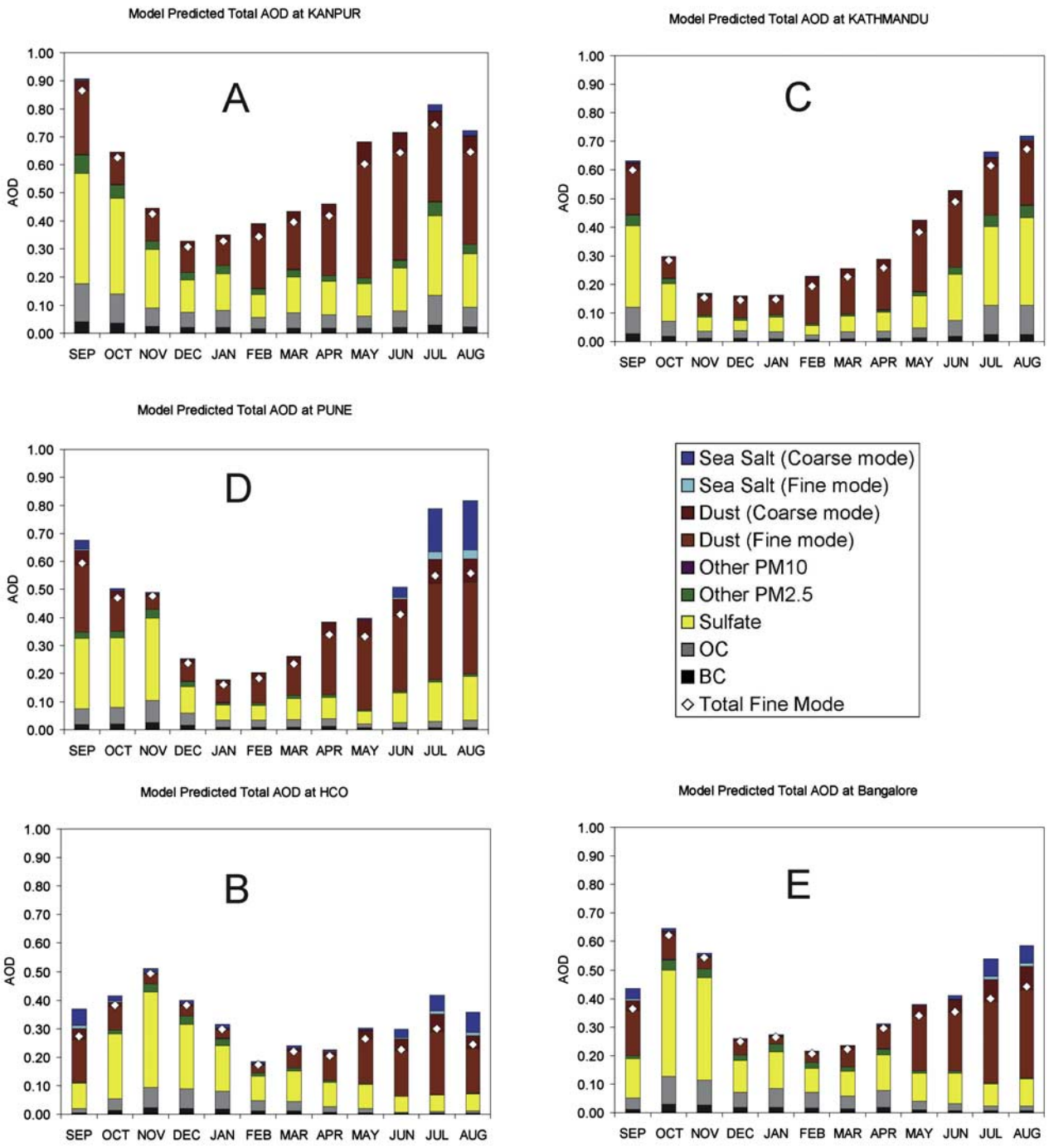

Figure 16. Individual aerosol contribution to total aerosol optical depth (AOD) predicted by the sulfur transport deposition model (STEM) for (a) Kanpur, (b) HCO, (c) KTM, (d) Pune, and (e) Bangalore.

available vertical aerosol observation data for the study period. As south Asian aerosol vertical profile becomes available, it will reduce model uncertainties in future modeling studies. The study has constrained the emissions of dust using $PM_{2.5}$ and PM_{10} observation from two sites. Observations of dust concentration from the interior south Asian continent would help in further constraining the dust emissions and modeling study. The model would be better constrained from more anthropogenic aerosol observations throughout south Asia.

5. Summary

[56] The STEM model has been used to study the seasonality, composition, and spatial distribution of major anthropogenic aerosols over south Asia. The modeling study was conducted at 50 km by 50 km resolution for 1

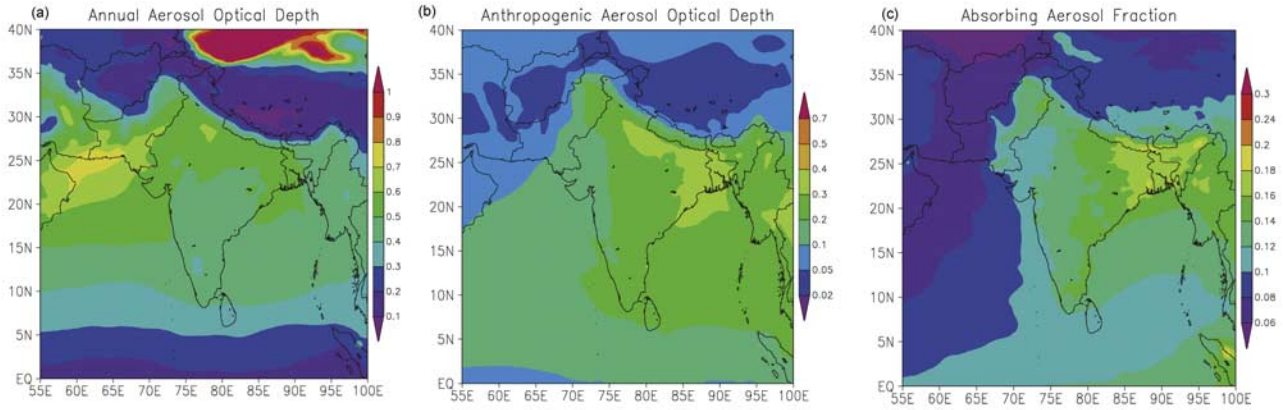

Figure 17. (a) Annual aerosol optical depth, (b) anthropogenic aerosol optical depth, and (c) absorbing aerosol contribution to anthropogenic aerosol optical depth over south Asia from 1 September 2004 to 31 August 2005.

a with three-hourly meteorological outputs from a regional simulation using MM5. Constrained by the NCEP/NCAR global reanalysis large-scale circulation using nudging, the regional simulation reproduced a realistic synoptic variability and seasonal distribution of winds and precipitation for modeling aerosol. However, the model has a dry bias for precipitation during the summer monsoon and postmonsoonal months.

[57] The aerosol model predictions are compared with yearlong data obtained from the Atmospheric Brown Cloud (ABC) project. The model is able to capture the magnitude and seasonality of sulfate, BC, and OC aerosols at the ABC-Hanimaadhoo observatory. The model captures the mean annual concentration over KTM but presently is not able to explain the high-aerosol peak in the dry months. The model is able to capture some of the seasonal trends and magnitude of AERONET AOD observations at Kanpur and AOD observations from the ABC project.

[58] The results show that the aerosol concentration over Hanimaadhoo is at its peak during the early dry season when winds are northerly and bring polluted air from south India. During these months the windblown dust and sea salt concentration are at a minimum, hence the percentage of anthropogenic aerosol composition is higher than 80 percent; this can be compared to wet monsoonal months when anthropogenic aerosol percentage is less than 20 percent. While the month of February still sees a significant amount of pollution over Maldives, the north Indian states see a minimum aerosol loading. The peak aerosol loading directly over the Ganges valley is seen in September while wider spatial spread is seen in the postmonsoonal transition period. The modeling results show that the Ganges valley experiences high-anthropogenic aerosol loading during the monsoon months, which is supported by AOD observations at Kanpur, but needs to be more thoroughly corroborated by future experimental campaigns.

[59] Comparison of predictions with observations also points out areas where model improvements are needed. For example, the sulfate comparison shows that the model consistently underpredicts the observations during the dry months, suggesting that the current sulfate production parameterization needs to be reevaluated for the south Asian region during the dry season.

[60] Finally, fine-mode AOD is shown to contribute significantly to total AOD during the postmonsoonal months (October–November) at most cities analyzed. Sulfate contribution to annual anthropogenic AOD is high at all the cities discussed along with greater than 10% contribution from absorbing aerosols. The late dry season (March–May) sees a substantial contribution of dust over all of south Asia.

[61] Emissions are a large source of uncertainty; the results support the need for improved emissions inventory. In addition to the brick kiln emissions in Kathmandu, open biomass burning is also a significant source of uncertainty.

[62] More experimental measurements of natural and anthropogenic aerosols such as sulfate, BC, OC, sea salt, and windblown dust along with measurements of trace gases such as ozone, SO_2, and CO over the Indian subcontinent are necessary to constrain the model and improve our understanding of the south Asian aerosols. Vertical profiles of these aerosol and trace gases over south Asia will help further constrain the model.

[63] **Acknowledgments.** We thank Brent Holben and Ramesh P. Singh for their effort in establishing and maintaining the AERONET Kanpur site so that we can use their AOT data. We would also like to thank our reviewers for their helpful suggestions. This work was supported by ABC related grants from NOAA and NASA.

References

Babu, S. S., S. K. Satheesh, and K. Krishna Moorthy (2002), Aerosol radiative forcing due to enhanced black carbon at an urban site in India, *Geophys. Res. Lett.*, *29*(18), 1880, doi:10.1029/2002GL015826.

Bates, T. S., et al. (2006), Aerosol direct radiative effects over the northwest Atlantic, northwest Pacific, and north Indian Oceans: Estimates based on in-situ chemical and optical measurements and chemical transport modeling, *Atmos. Chem. Phys.*, *6*, 1657–1732.

Cadle, S. H., and J. M. Dasch (1988), Wintertime concentrations and sinks of atmospheric particulate carbon at a rural location in northern Michigan, *Atmos. Environ.*, *22*, 1373–1381.

Carmichael, G. R., et al. (2003), Regional-scale chemical transport modeling in support of the analysis of observations obtained during the TRACE-P experiment, *J. Geophys. Res.*, *108*(D21), 8823, doi:10.1029/2002JD003117.

Carrico, C. M., et al. (2003), The importance of carbon and mineral dust to seasonal aerosol properties in the Nepal Himalaya, *Atmos. Environ.*, *37*, 2811–2824.

Chameides, W. L., et al. (1999), Case study of the effects of atmospheric aerosols and regional haze on agriculture: An opportunity to enhance crop yields in China through emission controls?, *Proc. Natl. Acad. Sci. U. S. A.*, *96*, 13,626–13,633.

Chung, S. H., and J. H. Seinfeld (2002), Global distribution and climate forcing of carbonaceous aerosols, *J. Geophys. Res.*, *107*(D19), 4407, doi:10.1029/2001JD001397.

Cooke, W. F., and J. J. N. Wilson (1996), A global black carbon aerosol model, *J. Geophys. Res.*, *101*, 19,395–19,409.

Gong, S. L. (2003), A parameterization of sea-salt aerosol source function for sub- and super-micron particles, *Global Biogeochem. Cycles*, *17*(4), 1097, doi:10.1029/2003GB002079.

Grell, G., et al. (1995), A description of the fifth generation Penn State/NCAR mesoscale model (mm5), *NCAR Tech. Note NCAR/TN-398+IA*, 107 pp., Natl. Cent. for Atmos. Res., Colo.

Guttikunda, S. K., Y. Tang, G. R. Carmichael, G. Kurata, L. Pan, D. G. Streets, J.-H. Woo, N. Thongboonchoo, and A. Fried (2005), Impacts of Asian megacity emissions on regional air quality during spring 2001, *J. Geophys. Res.*, *110*, D20301, doi:10.1029/2004JD004921.

Huffman, G. J., et al. (2001), Global precipitation at one-degree daily resolution from multisatellite observations, *J. Hydrometeorol.*, *2*, 36–50.

Koch, D. (2001), Transport and direct radiative forcing of carbonaceous and sulfate aerosols in the GISS GCM, *J. Geophys. Res.*, *106*, 20,311–20,332.

Leung, L. R., et al. (2003), Hydroclimate of the western United States based on observations and regional climate simulation of 1981–2000. Part I: Seasonal Statistics, *J. Clim.*, *16*, 1892–1911.

Liousse, C., et al. (1996), A global three-dimensional model study of carbonaceous aerosols, *J. Geophys. Res.*, *101*, 19,411–19,432.

Mayol-Bracero, O. L., R. Gabriel, M. O. Andreae, T. W. Kirchstetter, T. Novakov, J. Ogren, P. Sheridan, and D. G. Streets (2002), Carbonaceous aerosols over the Indian Ocean during the Indian Ocean Experiment (INDOEX): Chemical characterization, optical properties, and probable sources, *J. Geophys. Res.*, *107*(D19), 8030, doi:10.1029/2000JD000039.

Minvielle, F., et al. (2004a), Modelling the transport of aerosols during INDOEX 1999 and comparison with experimental data: 1. Carbonaceous aerosol distribution, *Atmos. Environ.*, *38*, 1811–1822.

Minvielle, F., et al. (2004b), Modelling the transport of aerosols during INDOEX 1999 and comparison with experimental data. Part 2: Continental aerosols and their optical depth, *Atmos. Environ.*, *38*, 1823–1837.

Moorthy, K. K., et al. (2005), Wintertime spatial characteristics of boundary layer aerosols over peninsular India, *J. Geophys. Res.*, *110*, D08207, doi:10.1029/2004JD005520.

Novakov, T., et al. (2000), Origin of carbonaceous aerosols over the tropical Indian Ocean: Biomass burning or fossil fuels?, *Geophys. Res. Lett.*, *27*, 4061–4064.

Olivier, J. G. J., and J. J. M. Berdowski (2001), Global emissions sources and sinks, in *The Climate System*, edited by J. Berdowski et al., pp. 33–78, A. A. Balkema, Lisse, Neth.

Parashar, D. C., et al. (2005), Carbonaceous aerosol emissions from India, *Atmos. Environ.*, *39*, 7861–7871.

Penner, J. E., et al. (1993), Towards the development of a global inventory for black carbon emissions, *Atmos. Environ., Part A*, *27*, 1277–1295.

Penner, J. E., et al. (2001), Aerosols, their direct and indirect effects, in *Climate Change 2001: The Scientific Basis: Contribution of Working Group I to the Third Assessment Report of the Intergovernmental Panel on Climate Change*, edited by J. T. Houghton et al., chapter 5, Cambridge Univ. Press, New York.

Pope, C. A., III, et al. (2002), Lung cancer, cardiopulmonary mortality, and long-term exposure to fine particulate air pollution, *J. Am. Medical Assoc.*, *287*, 1132–1141.

Pope, C. A., et al. (2006), Ischemic heart disease events triggered by short-term exposure to fine particulate air pollution, *Circulation*, *114*, 2443–2448.

Qian, Y., and L. R. Leung (2007), A long-term regional simulation and observations of the hydroclimate in China, *J. Geophys. Res.*, *112*, D14104, doi:10.1029/2006JD008134.

Ramana, M. V., and V. Ramanathan (2006), Abrupt transition from natural to anthropogenic aerosol radiative forcing: Observations at the ABC-Maldives Climate Observatory, *J. Geophys. Res.*, *111*, D20207, doi:10.1029/2006JD007063.

Ramanathan, V., et al. (2001a), Atmosphere aerosols, climate, and the hydrological cycle, *Science*, *294*, 2119–2124.

Ramanathan, V., et al. (2001b), Indian Ocean experiment: An integrated analysis of the climate forcing and effects of the great Indo-Asian haze, *J. Geophys. Res.*, *106*, 28,371–28,398.

Ramanathan, V., et al. (2005), Atmospheric brown clouds: Impacts of south Asian climate and hydrological cycle, *Proc. Natl. Acad. Sci., U. S. A.*, *102*, 5326–5333.

Ramanathan, V., et al. (2007), Atmospheric brown clouds: Hemispherical and regional variations in long range transport, absorption and radiative forcing, *J. Geophys. Res.*, *112*, D22S21, doi:10.1029/2006JD008124.

Rastogi, N., and M. M. Sarin (2005), Chemical characteristics of individual rain events from a semi-arid region in India: Three-year study, *Atmos. Environ.*, *39*, 3313–3323.

Reddy, M. S., and O. Boucher (2004), A study of the global cycle of carbonaceous aerosols in the LMDZT general circulation model, *J. Geophys. Res.*, *109*, D14202, doi:10.1029/2003JD004048.

Reddy, M. S., and C. Venkataraman (2002), Inventory of aerosol and sulphur dioxide emissions from India: I. Fossil fuel combustion, *Atmos. Environ.*, *36*, 677–697.

Reddy, M. S., O. Boucher, C. Venkataraman, S. Verma, J.-F. Léon, N. Bellouin, and M. Pham (2004), General circulation model estimates of aerosol transport and radiative forcing during the Indian Ocean Experiment, *J. Geophys. Res.*, *109*, D16205, doi:10.1029/2004JD004557.

Stone, E., G. C. Lough, J. Schauer, P. Siva, C. Corrigan, and V. Ramanathan (2007), Understanding the origin of black carbon in the atmospheric brown cloud over the Indian Ocean, *J. Geophys. Res.*, *112*, D22S23, doi:10.1029/2006JD008118.

Streets, D. G., et al. (2003), An inventory of gaseous and primary aerosol emissions in Asia in the year 2000, *J. Geophys. Res.*, *108*(D21), 8809, doi:10.1029/2002JD003093.

Sumanth, E., K. Mallikarjuna, J. Stephen, M. Moole, V. Vinoj, S. K. Satheesh, and K. K. Moorthy (2004), Measurements of aerosol optical depths and black carbon over Bay of Bengal during post-monsoon season, *Geophys. Res. Lett.*, *31*, L16115, doi:10.1029/2004GL020681.

Tang, Y., et al. (2004), Impacts of dust on regional tropospheric chemistry during the ACE-Asia experiment: A model study with observations, *J. Geophys. Res.*, *109*, D19S21, doi:10.1029/2003JD003806.

Tang, Y., et al. (2007), Influence of lateral and top boundary conditions on regional air quality prediction: A multiscale study coupling regional and global chemical transport models, *J. Geophys. Res.*, *112*, D10S18, doi:10.1029/2006JD007515.

United Nations Environment Programme and the Center for Clouds, Chemistry and Climate (UNEP and C^4) (2002), *The Asian Brown Cloud: Climate and other Environmental Impacts*, U. N. Environ. Programme, Nairobi, Kenya.

Uno, I., G. R. Carmichael, D. Streets, S. Satake, T. Takemura, J. Woo, M. Uematsu, and S. Ohta (2003a), Analysis of surface black carbon distributions during ACE-Asia using a regional-scale aerosol model, *J. Geophys. Res.*, *108*(D23), 8636, doi:10.1029/2002JD003252.

Uno, I., et al. (2003b), Regional chemical weather forecasting system CFORS: Model descriptions and analysis of surface observations at Japanese island stations during the ACE-Asia experiment, *J. Geophys. Res.*, *108*(D23), 8668, doi:10.1029/2002JD002845.

Uno, I., et al. (2004), Numerical study of Asian dust transport during the springtime of 2001 simulated with the Chemical Weather Forecasting System (CFORS) model, *J. Geophys. Res.*, *109*, D19S24, doi:10.1029/2003JD004222.

Venkataraman, C., et al. (2005), Residential biofuels in south Asia: Carbonaceous aerosol emissions and climate impacts, *Science*, *307*, 1454–1456.

Walcek, C. J., et al. (1986), Sulfur dioxide, sulfate and nitric acid deposition velocities computed using regional land use and meteorological data, *Atmos. Environ.*, *20*, 949–964.

Wesely, M. L., and B. B. Hicks (2000), A review of the current status of knowledge on dry deposition, *Atmos. Environ.*, *34*, 2261–2282.

Zhang, M. (2004), Modeling of organic carbon aerosol distributions over east Asia in the springtime, *China Particuol.*, *2*, 192–195.

B. Adhikary, 407 IATL, Iowa City, IA 52242, USA. (adhikary@cgrer.uiowa.edu)

G. R. Carmichael, 401 IATL, Iowa City, IA 52242, USA. (gcarmich@engineering.uiowa.edu)

L. R. Leung and Y. Qian, Pacific Northwest National Laboratory, P.O. Box 999, Richland, WA 99352, USA. (ruby.leung@pnl.gov; yun.qian@pnl.gov)

M. V. Ramana and V. Ramanathan, Center for Atmospheric Sciences, SCRIPPS Institute of Oceanography, University of California at San Diego, 9500 Gilman Drive, La Jolla, CA 92093, USA. (vramanathan@ucsd.edu; ramana@fiji.ucsd.edu)

J. J. Schauer and E. A. Stone, Environmental Chemistry and Technology Program, University of Wisconsin-Madison, Madison, WI 53706, USA. (jjschauer@wisc.edu; eastone@wisc.edu)

Y. Tang, 402 IATL, Iowa City, IA 52242, USA. (ytang@cgrer.uiowa.edu)